Macromolecules

pubs.acs.org/Macromolecules Perspective

Providing a Window into the Phase Behavior of Semiconducting Polymers

Ioan Botiz, Marlow M. Durbin, and Natalie Stingelin*

Cite This: *Macromolecules* 2021, 54, 5304–5320 Read Online

ABSTRACT: The targeted assembly of a wealth of functional architectures for soft photonics and electronics relies on a rigorous understanding of semiconducting polymer phase behavior. While many useful correlations have been established in the field of commodity plastics, unifying theories for their semiconducting counterparts are, however, more challenging to develop because of the rich phase behavior frequently displayed by these macromolecules, due in part to their complex chemical structures typically based on relatively rigid backbones and elaborate side-chain motifs. Solid-state structure formation and resulting properties are therefore especially sensitive to thermal and temporal parameters during processing, rendering device fabrication a challenging task that too often relies on time-consuming trial-and-error procedures. To understand the thermodynamic and kinetic factors of plastic semiconductor solidification and, for example, thin-film growth relevant for device fabrication, detailed knowledge of the intricacies of macromolecular semiconductors' phase behavior must be gained and ideally combined with temperature/composition, temperature/confinement, and/or time/temperature/transformation- phase diagrams. This will open pathways toward a knowledge and methodology platform for the controlled materials assembly of soft electronics/photonics systems very much in analogy to the approaches used in metallurgy and the inorganic electronic materials field. In turn, a step change in how we design and process soft electronic products might be achieved, with impact on the broader soft matter area.

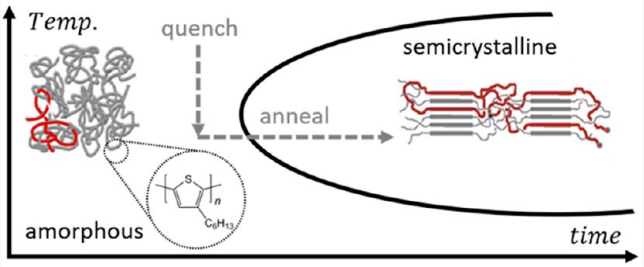

INTRODUCTION

Semiconducting polymers are generally based on π-conjugated macromolecules featuring alternating single and double bonds between sp^2-hybridized carbon atoms or heteroatoms.[1,2] Unique among plastic materials for their electrical conductivity/semiconductivity, combined often with distinctive optical properties such as light emission, this special class of functional polymers has attracted significant interest for next-generation electronic and optoelectronic devices, from organic light-emitting diodes to organic photovoltaics and, for example, soft electrodes for bioelectronics applications. Like all polymers, semiconducting polymers display properties that are dependent on their molecular weight, molecular weight distribution, and chemical structure.[3−5] In semiconducting plastics, backbone rigidity and conformation (planarity versus torsional disorder) and selected side-chain motifs additionally play critical roles. Hence, there is a large set of factors that strongly influence polymer assembly along with various physical parameters including melting (T_m), crystallization (T_c), and glass-transition (T_g) temperatures, side-chain softening,[6] and, potentially, liquid-crystalline phase transitions. As a consequence, to gain full control over the solid-state structure development of this class of macromolecules, it is essential to obtain a detailed picture of their thermal phase behavior. Here, we deliver a perspective on specific processes and physicochemical parameters dictating the thermal phase behavior of semiconducting plastics and on methodologies that have been shown to be powerful for their characterization, including use of experimentally established nonequilibrium temperature/composition phase diagrams and time/temperature/transformation diagrams. A detailed picture of the thermal phase behavior of these complex systems, established with such a methodology set, can be expected to enable formation of targeted semiconducting polymer architectures exhibiting desired optoelectronic characteristics and device performances. For this we need to build on the knowledge gained in the commodity polymer area and, more broadly, the general materials science field.

Received: February 7, 2021
Revised: June 1, 2021
Published: June 9, 2021

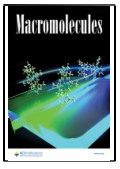

https://doi.org/10.1021/acs.macromol.1c00296
Macromolecules 2021, 54, 5304–5320

MOLECULAR WEIGHT, CHAIN CONFORMATION, AND CHAIN ENTANGLEMENT

The majority of the new generation of polymer semiconductors feature relatively low molecular weight and rigid backbones. This has a significant effect on phase transitions such as melting and crystallization.[7] One reason is that both attributes (molecular weight, backbone rigidity) influence the number of entanglements that can occur per chain, which in turn affects macromolecular assembly. More specifically, flexible-chain polymers of high molecular weight, such as many commodity plastics and some semiflexible-chain semiconductors like poly(3-hexylthiophene) (P3HT), are characterized by a high (Figure 1a, left) or intermediate (Figure 1a, middle) entanglement density, especially when processed from the melt.[7] In contrast, in rigid-rod-like polymers (Figure 1a, right), such as new-generation plastic semiconductors,[6,8] a far smaller number of entanglements form, if any. Accordingly, the molecular weight between entanglements, M_e (indicated in Figure 1b), often becomes larger than the molecules' length, meaning no chain entanglement can occur. This can strongly affect the material's solid-state structure development as well as the phase behavior of the resulting architectures, as the number of entanglements per chain affects their segmental mobility and, thus, parameters such as mass transport.[9,10]

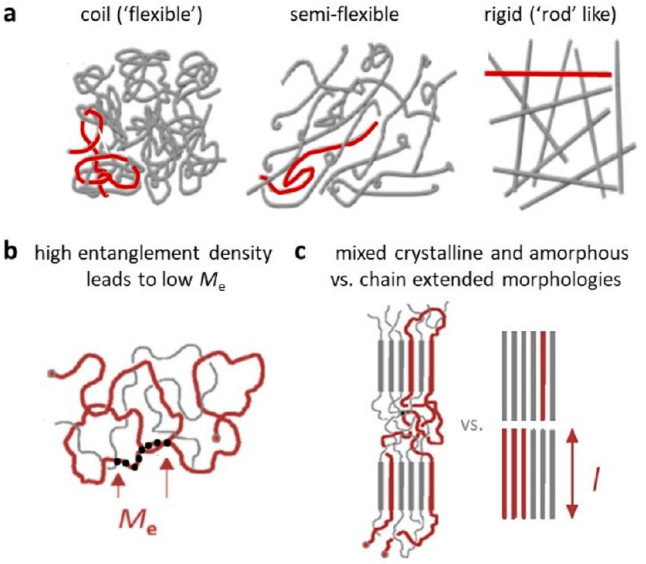

Figure 1. (a) Macromolecules can adopt a wide variety of conformations depending on the backbone flexibility/rigidity. (b) Representation of an entangled polymer melt or solution, where the molecular weight between entanglements, M_e, important for the solid-state structure development, is indicated. (c) Schematic representations of a two-phase morphology composed of interlinked crystalline lamellae and entangled amorphous regions (left) compared to a chain-extended crystal where the crystal thickness, l, equals the polymer chain length (right). Adapted from ref 13.

In most classical polymers as well as first-generation semiconductors such as P3HT, where typically a large number of entanglements develop per polymer chain and, thus, M_e is small, a solid-state microstructure consisting of interconnected crystalline lamellae alternating with largely disordered (amorphous) regions form (Figure 1c, left).[7,11,12] In strong contrast, if the molecular weight M (given, for example, by the weight-average molecular weight, M_w) is smaller than M_e, readily achieved in rigid-rod-chain polymers, solid-state structures composed of disconnected, chain-extended crystals develop (Figure 1c, right).[8]

Which specific solid-state structure—chain-extended crystals versus two-phase morphology of interconnected crystalline moieties embedded within an amorphous "matrix"—is developed by a given polymer/processing scenario can be experimentally identified by employing techniques such as thermal analysis (Figure 2). The reason is that T_m is directly correlated to the lamellar thickness, l, of the crystals that form (chain-extended or interconnected). This can be described by the Gibbs–Thomson equation.[14,15] For semiflexible-chain materials of low M_w as well as rigid-rod-like polymers (low and high M_w), l will increase with molecular weight and

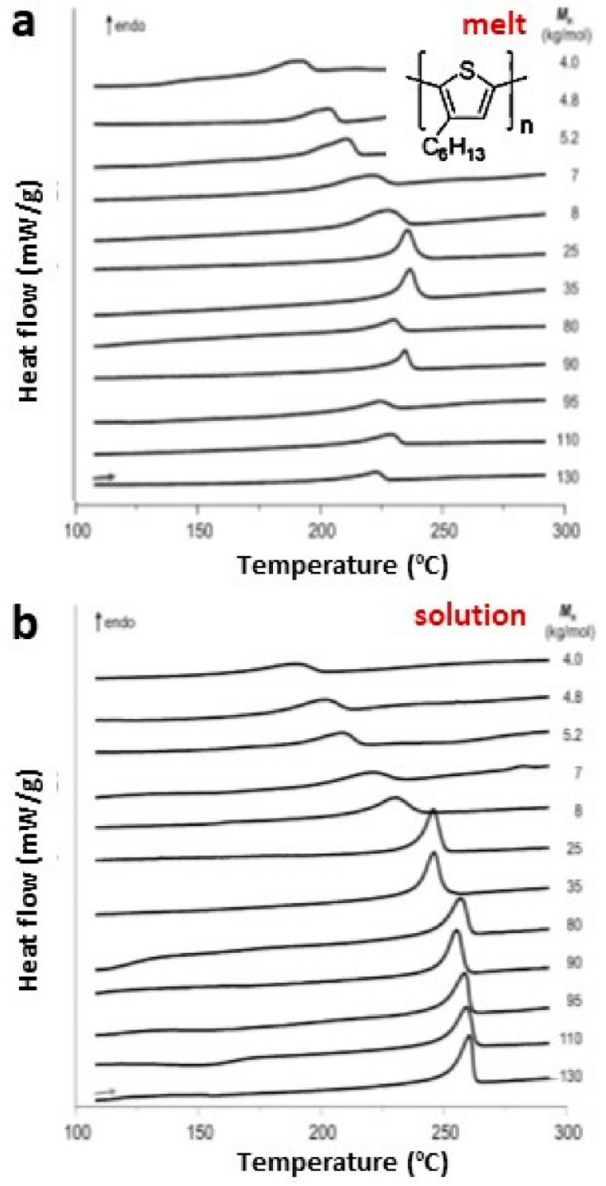

Figure 2. (a) Differential scanning calorimetry (DSC) heating thermograms measured with a heating rate of 10 °C/min for melt-solidified P3HT samples of a range of molecular weights (values given next to the thermograms, given here with the number-average molecular weight, M_n). (b) Corresponding DSC heating thermograms measured for solution-cast P3HT films. Adapted from ref 7.

https://doi.org/10.1021/acs.macromol.1c00296
Macromolecules 2021, 54, 5304−5320

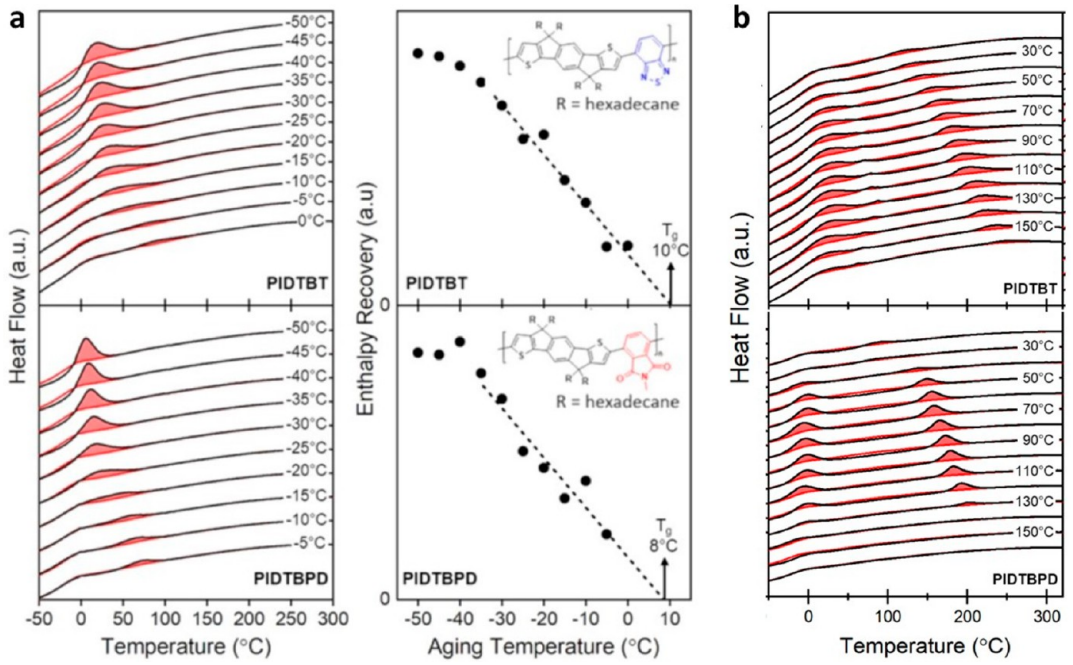

Figure 3. (a) Left: fast differential scanning calorimetry (F-DSC) heating thermograms comparing aged (black) and unaged (red) PIDTBT (top panel) and PIDTBPD (bottom panel). Enthalpic overshoots (red highlighted areas) are observed when the aging temperatures (indicated on the right of the graph) were below the glass transition temperature of the materials (see for details refs 6, 38, and 39). Right: extrapolating the enthalpy recovery between aged and unaged samples of PIDTBT and PIDTBPD (top and bottom panel, respectively) allows determination of the temperature at which the enthalpy overshoot is zero. This temperature correlates to the onset of the glass transition temperature, i.e., the temperature at which vitrification sets in upon cooling. (b) Two distinct endotherms appear when annealing samples above the glass transition temperatures, indicating possible liquid-crystalline or liquid-crystalline-like transitions. For PIDTBPD, the first transition thereby occurs at temperatures notably below room temperature (around 0 °C), while for PIDTBT the transition is around room temperature with a tail reaching 100 °C. Adapted from ref 6.

eventually reach the length of the constituting macromolecules. As a consequence, T_m essentially linearly increases with M_w as well, as observed for the semiflexible semiconductor P3HT when processed from the melt.[7,11] For high-M_w, semiflexible-chain materials once the polymer chains start to entangle at sufficiently high molecular weights, which generally is only found for flexible- and semiflexible-chain macromolecules, intertwining and folding occur, similar to most classical polymers.[16,17] This typically leads to crystalline moieties of a thickness l smaller than the chain length of the constituting molecules.[7,11,18] Accordingly, T_m decreases once entanglements form (Figure 2a).[7]

This behavior can be manipulated by processing the flexible-chain polymer semiconductor from solution. The presence of a solvent leads to a reduction in the number of entanglements as a function of solution composition/concentration and the quality of the solvent. This has a significant effect especially for materials of high M_w, where the decrease in number of entanglements upon dilution results in an increase of l, and thus in an increase of T_m, as exemplified by the thermograms measured for solution-processed P3HT (Figure 2b).[7] Very similar to commodity plastics, in the extreme case of highly diluted solutions single crystals can be produced,[19] where the number of initial nuclei can be controlled through self-seeding as was shown on P3HT, with the crystals exhibiting unusual light absorption and highly anisotropic charge transport properties.[20,21]

Other important observations can be made on the example of P3HT that can be translated to many new-generation materials that usually are of a notably lower entanglement density because of their more rigid backbone compared to P3HT. Specifically, for P3HT of low M_w, reduced enthalpies of fusion are measured compared to longer-chain materials. This suggests that the structural order in these P3HTs is lower. Likely, end groups hinder chain packing despite the fact that in such low-M_w systems, due to the low entanglement density, the macromolecular chains have relatively high mobility leading to increased mass transport,[7,11] which in many other scenarios would help formation of crystalline moieties.[7,11] Similarly, chain defects such as region defects in the polymer backbone can hinder chain packing and, in turn, may affect the polymer's phase behavior.[22]

The enhanced molecular mobility in low-molecular-weight materials can, moreover, lead to morphological instabilities.[23] In hexylthiophene oligomers, for instance, various polymorphs were identified, which varied in the macromolecular tilt within the crystalline moieties, leading to different arrangements within one architecture.[24] This has a drastic effect on the local optoelectronic properties and can be expected to be more pronounced in more rigid-rod-like polymers, which often are of low molecular weight.

Various experimental conditions, including exposure of the material to high temperatures and/or pressure, can furthermore be exploited to direct the final shape and degree of perfection of the crystalline entities in polymeric semiconductors, including their lamellar crystal thickness l. For instance, similar to commodity polymers such as polyethylene, crystallization at elevated temperatures can lead to crystalline entities of increased thicknesses.[25−27] This was demonstrated on solution-grown poly(thiophene) derivatives,[28] with pro-

https://doi.org/10.1021/acs.macromol.1c00296
Macromolecules 2021, 54, 5304−5320

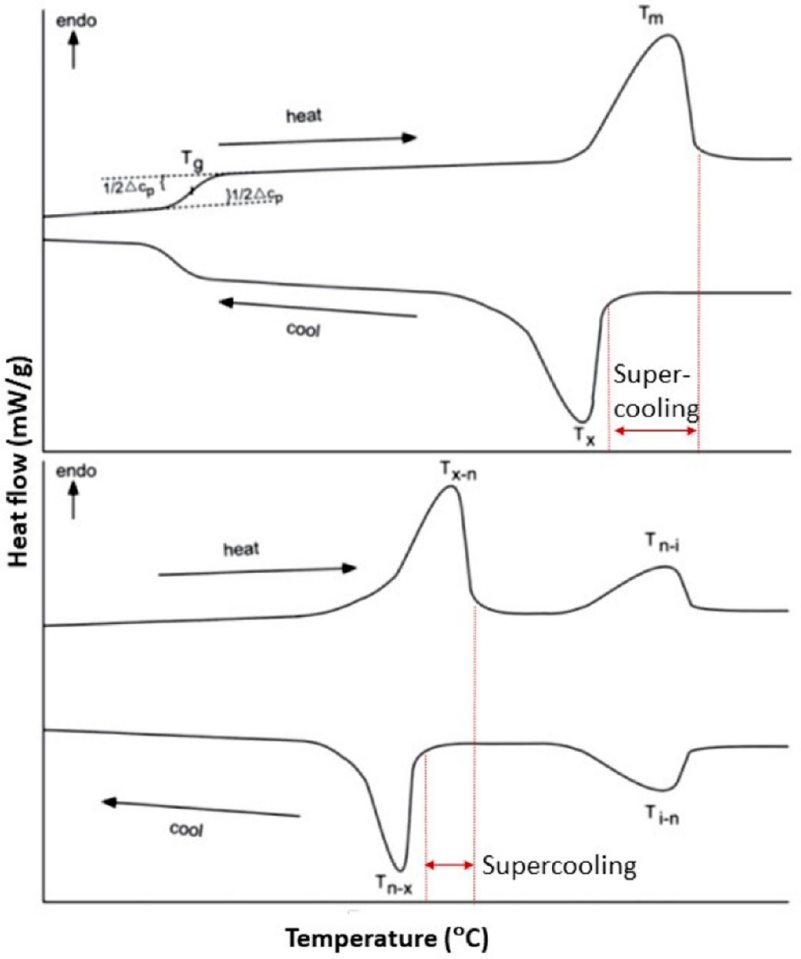

Figure 4. (top) Differential scanning calorimetry (DSC) heating and cooling thermograms for a typical semicrystalline polymer with a well-developed glass transition T_g, and a clean melting endotherm (T_m) upon heating; upon cooling, a crystallization exotherm (T_x) is observed. Generally, a large supercooling, $\Delta T = T_m - T_x$, is needed for the material to solidify, especially for highly entangled samples. (bottom) Materials that display liquid-crystalline phases, here given with an exemplary transition from a crystalline to a liquid-crystalline phase denoted T_{x-n} and an isotropic melting at T_{n-i}, display typically a small supercooling (here: the difference between $T_{n-i} - T_{i-n}$), while the one between the liquid-crystalline and the crystalline phase (i.e., $T_{x-n} - T_{n-x}$) may be more pronounced. Adapted from ref 36.

nounced effects on the yield and dynamics of the photogenerated charge carriers. Even more efficiently, crystallization under high pressure has led to P3HT structures of nearly fully extended-chain crystals,[29] resulting in excellent bulk charge transport. The exposure of other conjugated polymers such as polyfluorenes (PFOs) to high pressure was also shown to induce notable changes to l, resulting in variations in the chain conformation and, in turn, a red-shifted photoluminescence.[30] The interchain distance was reduced as well.[31]

The situation becomes more complex when we transition from semiflexible-chain semiconductors, such as P3HT, where many classical polymer science tools established for materials such as polyethylene and polypropylene can be applied, to more recent, rigid-rod-like polymers, such as poly[2,5-bis(3-tetradecylthiophen-2-yl)thieno[3,2-*b*]thiophene] (PBTTT),[9,32,33] or materials based on indacenodithiophene (IDT)—a widely used structural motif in organic electronics, where three conjugated aromatic rings are fixed in a coplanar nature by bridging atoms between these rings to ensure linear backbones (planar or torsionally disordered) with good orbital delocalization across the IDT unit.[6,34,35]

The linear, rod-like character of the backbone critically dictates the thermal phase behavior of these functional plastics, including phase transitions such as melting and glass transition, which can be further manipulated by the selection of a specific side-chain motif (see, for example, Figure 3). More specifically, an increase in polymer backbone rigidity leads to smaller conformational changes between the liquid and the solid state; hence, the change in entropy of fusion is low. Because T_m is proportional to the change in enthalpy of fusion while being inversely proportional to the change in entropy of fusion,[13] this renders T_m to be high.[36,37] On the other hand, because of the more plastic-crystal-like behavior, resulting from the small difference in the enthalpy of fusion of the solid and liquid state,[37] many plastic semiconductors experience a rich phase behavior,[9] including the occurrence of liquid-crystalline (LC) phases such as thermotropic (LC phases in the solid state) or lyotropic (solution LC phases) phases with high degree of order along at least one molecular direction. Moreover, some liquid-crystalline-like features can occur, especially above the side-chain softening temperature, having shown in some IDT-based polymers to dominate mechanical and electronic characteristics.[6]

A challenge in analyzing LC phases as well as side chain softening temperatures is that they can be difficult to detect experimentally. It is often intricate, for instance, to distinguish

https://doi.org/10.1021/acs.macromol.1c00296
Macromolecules 2021, 54, 5304−5320

between LC-phase transitions, solid−solid crystalline transformations, and melting/crystallization processes. In the case of polymeric species, differentiation between melting/crystallization and LC-mesophase transitions may be achieved based on how large the magnitude of supercooling is (Figure 4) because small supercooling generally can be attributed to LC-mesophase transitions while crystallization usually requires a pronounced supercooling in polymeric species.[36]

To better understand LC phases, for example, uniaxial (nematic) mesoscopically ordered structures specific to, for example, rod-like poly(alkoxyphenylenevinylene)[40] and to semiflexible poly(alkylthiophenes),[40] a number of theoretical models may be employed.[40−46] If the analysis of the phase behavior of conjugated polymers becomes more complex, especially when LC phases or LC-like phases above the side-chain softening are "hidden" behind other endothermic processes,[9,10,47−50] fast differential scanning calorimetry (F-DSC) can in some scenarios be useful.[6,38,39] F-DSC is uniquely equipped to mimic the kinetics of practical processing conditions such as spin coating and permits measurements of thin films of 100 nm thickness and less. It moreover enables elucidation of the crystallization dynamics and (meta)stability of systems in conditions far away from equilibrium,[51−57] as was shown on the organic, small-molecule semiconductor 7,7′-(4,4-bis(2-ethylhexyl)-4*H*-silolo[3,2-*b*:4,5-*b*′]dithiophene-2,6-diyl)bis(6-fluoro-4-(5′-hexyl[2,2′-bithiophen]-5-yl)benzo[*c*]-[1,2,5]thiadiazole) (p-DTS(FBTTh$_2$)$_2$).[58] F-DSC assisted in this case in identifying the metastable phases that this material can form, including a liquid crystalline transition, by utilizing ultrafast heating and cooling rates of a few thousand degrees Celsius per second to vitrify kinetically inhibited phase transitions while allowing transitions to occur that are not observable by conventional DSC (Figure 5).[51,58]

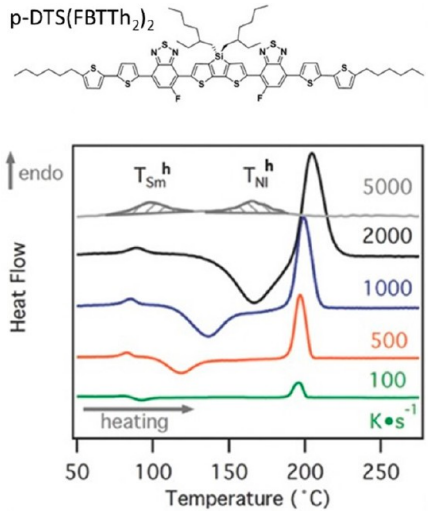

Figure 5. Fast differential scanning calorimetry measurements performed on the small-molecule semiconductor p-DTS(FBTTh$_2$)$_2$ at different heating rates, all from an initially vitrified state. At heating rates of 100−2000 °C/s, a weak endothermic transition is observed centered at 80 °C, attributed to a liquid crystalline phase transition (T_{Sm}^h) followed by an exothermic transition related to cold crystallization (i.e., crystallization in the solid state) of the material between 90 and 175 °C, depending on the heating rate. Finally a clear melting temperature endotherm is observed around 195−200 °C. In contrast, when a heating rate of 5000 °C/s was used, cold crystallization is prevented; instead, two endothermic transitions assigned to thermotropic smectic/nematic and nematic/isotropic mesophase transitions can be observed. The chemical structure of the p-DTS(FBTTh$_2$)$_2$ is shown in the top inset. Adapted from ref 58.

VITRIFICATION VERSUS CRYSTALLIZATION/MOLECULAR ORDERING

Because many recent polymer semiconductors are of a rather complex chemical design, their crystallization kinetics can be slow, hindering ordering during solidification. This effect is evident when quenching these materials from the liquid state, for example, during spin coating of a thin active layer for an optoelectronic device where solidification rates are kinetically ill-defined and are dictated mostly by the solvent evaporation rate. In this scenario, the rate of solidification can easily exceed that of molecular ordering. Thus, vitrification dominates; that is, a glass forms with highly suppressed segmental motion and a very limited degree of crystallinity.[12,18,59] This is especially common in many next-generation semiconductors, which, because of their complex chemical structure, are often forced into a state that is dominated by pronounced disorder over longer length scales, while some local order may persist. Postdeposition procedures might, in this scenario, be required to molecularly order such vitrified structures. This can, for instance, be done by annealing vitrified systems above the T_g, which leads to cold crystallization.[25,36]

Vitrification is a process that can, in some cases, indeed be intimately related to the glass transition of a polymer. As is the case in many commodity polymers, the thermal signature for the glass transition may, however, be ill defined and difficult to identify with traditional DSC methods that use relatively slow heating/cooling rates, on the order of a few degrees Celsius per minute, leading to a relatively low sensitivity. In this scenario, fast differential scanning calorimetry and oscillatory shear rheometry can be useful. F-DSC, on the one hand, displays exceptional sensitivity in measuring weak transitions such as glass transition temperatures and side-chain melting.[6] To identify T_g, the fast cooling rate of a few thousand degrees Celsius per second is exploited for the ultrarapid quenching into an essentially fully amorphous state that can be physically aged below its glass transition temperature or directly be reheated above the glass transition. Figure 3 displays, for instance, the heating thermograms for PIDTBT and PIDTBPD, two hairy-rod-like polymer semiconductors (see Figure 3 for their chemical structures) after aging, which leads to an enthalpic overshoot in a subsequent heating cycle (red shaded area) in case the aging temperature was below the glass transition temperature of the material, while corresponding reference thermograms recorded for samples immediately heated after quenching, without undergoing an aging step, do not show any overshoot.[6] Analyzing different aging temperatures, we can identify a lower aging temperature limit where no physical aging occurs and no enthalpic overshoot is recorded. This temperature is the onset of the glass transition regime.[6,38,39] On the other hand, parallel plate rheometry can reveal multiple relaxation signatures of glass transitions in conjugated polymers with relatively long side chains. Using cylindrical "puck" samples of regioregular and regiorandom P3HT, Xie et al., for example, demonstrated the distinct temperature dependence of low- and high-frequency relaxation processes attributed to respectively segmental backbone and side-chain motion.[60] Notably, this technique seems to overcome many of the challenges of dynamic mechanical analysis techniques—another elegant method for the identification of the glass transition regime that usually requires

https://doi.org/10.1021/acs.macromol.1c00296
Macromolecules 2021, 54, 5304−5320

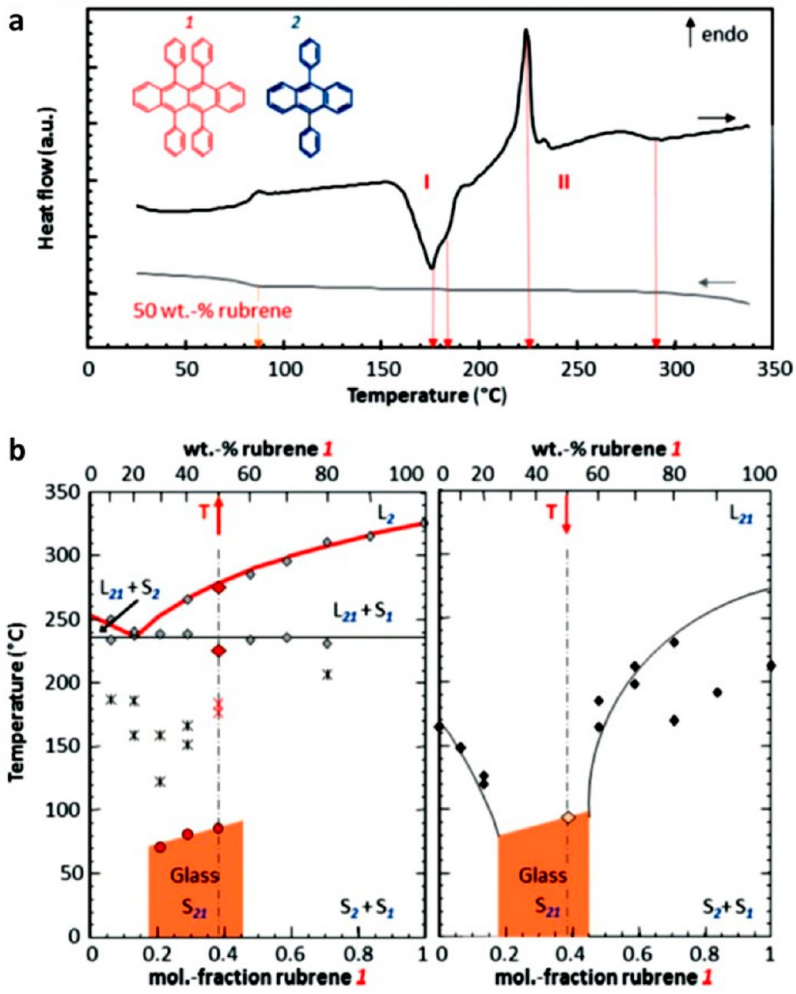

Figure 6. (a) DSC heating (black) and cooling (gray) thermograms of the diphenylanthracene:rubrene binary (50 wt % rubrene), from which the nonequilibrium phase diagrams, presented in (b), were constructed, as indicated by the red arrows. The data also allow regions to be identified where the initially amorphous film can be crystallized below and above the eutectic temperature (I and II). The inset shows the chemical structures of diphenylanthracene and rubrene. (b) Binary composition−temperature diagrams of the diphenylanthracene:rubrene system. Black solid symbols and crosses indicate crystallization temperatures; gray solid symbols represent melting and eutectic temperatures; red solid symbols are the measured glass transition temperatures. The liquidus curves for the heating diagram (left panel) can be calculated by using the equation for ideal solutions. Adapted from ref 63.

mounting of a thin film of the polymer of interest onto a reinforcing support structure.[61,62]

In some scenarios, vitrification of a material can be enhanced intentionally via the use of an additive—a so-called vitrifier—that hinders the crystallization of the semiconductor to induce a fully vitrified structure that is kinetically metastable. As a consequence, the initially glassy polymer films can be crystallized in a controlled manner in the solid state. Depending on the phase behavior of the conjugated polymer and the vitrifier, various crystallization routes may be accessed, allowing, for example, manipulation of the nucleation density, mass transport, and, generally, the crystallization rate and, thus, crystal size or crystal thickness, as shown on the small molecular semiconductor, rubrene (Figure 6).[63]

The vitrifier can be an active material. For instance, in spin-cast binary systems of P3HT and an electron acceptor commonly used in photovoltaics, that is, phenyl-C_{61}-butyric acid methyl ester (PCBM-C_{61}), blending followed by rapid solvent evaporation leads to fully vitrified films, while neat P3HT films still would exhibit some degree of crystallinity. However, annealing of the blend films above the T_g can induce cold crystallization of at least one blend component, followed by phase separation.[64−66] While partial phase separation improves the photovoltaic device performance, overcrystallization results in excessively strong phase separation and, in turn, to device degradation. Note: while in neat polymers a temperature above the single components' T_g should generally be employed for annealing, in blends, the T_g of the intermixed phase often provides the lower temperature limit for annealing.[64] When working with blends, it is thus critical to determine the T_g not only for each neat blend component but also for the intermixed phases.[39,64]

■ CONFINEMENT

It is worth emphasizing that specific chain conformations adopted by semiconducting polymers, or those of their small molecule counterparts, are a direct consequence of their chemical structure. Accordingly, the same material can often adopt an impressive number of chain conformations, especially in confined geometries like thin films, frequently with direct

https://doi.org/10.1021/acs.macromol.1c00296
Macromolecules 2021, 54, 5304−5320

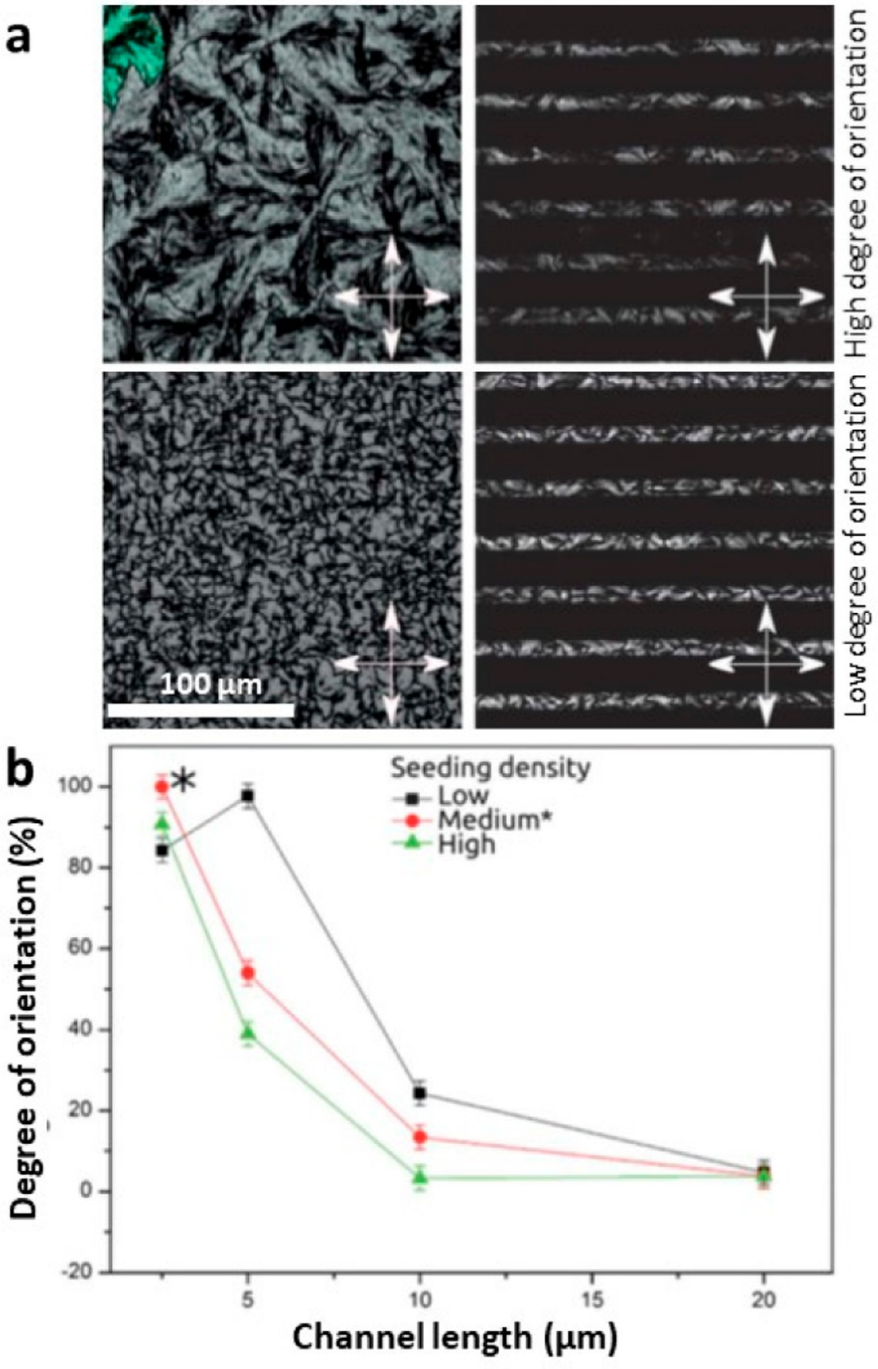

Figure 7. (a) Polarized optical micrographs of unconfined (left) and confined (right) crystalline P3HT spherulites. Top micrographs represent a low spherulite density while bottom micrographs correspond to a high spherulite density. (b) Degree of chain orientation relative to the sample with the highest chain orientation, marked with an asterisk, with respect to the channel length. Adapted from ref 70.

consequences to the material's optoelectronic properties. Because this effect strongly depends on environmental factors during solidification (e.g., substrate temperature, solution concentration, additives, and degree of confinement), film formation and, thus, device fabrication often suffer from low reliability and limited reproducibility.

Confinement also can drastically change the phase behavior of the polymer.[67−69] This is because in confined spaces the characteristic length scales of physical processes such as crystallization, phase separation, or conformational transitions are of a similar order of magnitude as the space available for these processes to occur. For example, in very thin films, as typically used in the fabrication of various optoelectronic devices, reorganization of the macromolecular chains necessary for the material to crystallize requires a volume that is equal to or larger than the volume provided by the film. Thus, the solidification behavior may be altered due to such size constraint compared to systems with no size limitation. For instance, intermolecular interactions between the polymer and substrate, and the physical presence of free surfaces, may affect the glass transition of polymers when, for example, in thin-film form. Furthermore, in a confined volume, the maximum extent

https://doi.org/10.1021/acs.macromol.1c00296
Macromolecules 2021, 54, 5304−5320

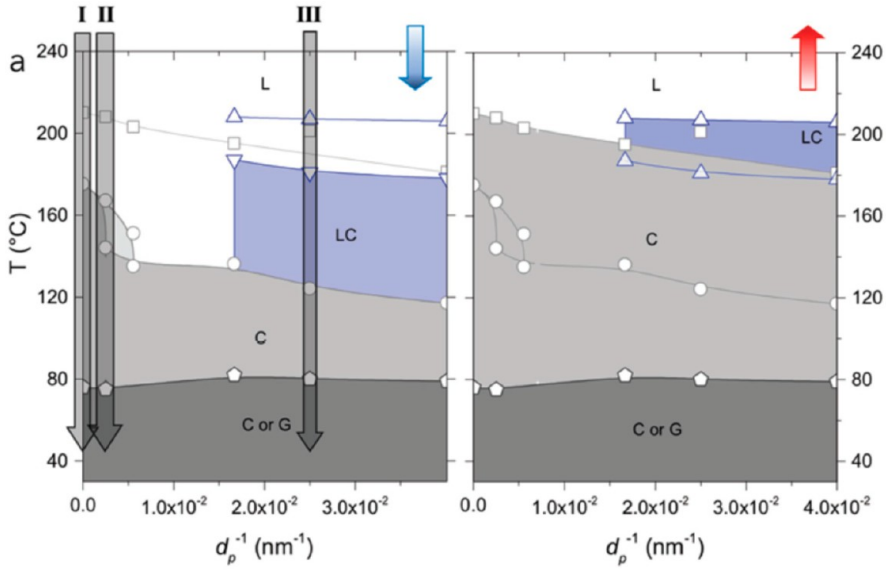

Figure 8. Temperature/confinement phase diagrams for p-DTS(FBTTh$_2$)$_2$ for cooling (left panel) and heating (right panel), where temperatures are plotted against inverse pore diameter in nanometers. Gray circles: crystallization temperatures; gray squares: melting temperatures; blue down-pointing triangles: mesophase formation; blue up-pointing triangles: mesophase melting; dark gray pentagons: glass transition temperatures. The dark-gray shading corresponds to the temperature/confinement region where p-DTS(FBTTh$_2$)$_2$ is in either a glassy or a crystalline state depending on the cooling rate applied. Light gray shading corresponds to the region where p-DTS(FBTTh$_2$)$_2$ exclusively is crystalline. Blue shading corresponds to conditions where a layered mesophase is formed, while the white region corresponds to the isotropic liquid. Cooling pathways I, II, and III are indicated. Adapted from ref 71.

of crystal growth may be limited in one or more directions by (film) geometry and/or by the number of nuclei forming in a confined volume, which typically is orders of magnitude lower than the number of nuclei found within the bulk of a polymer.[13,67] Because of the small number of nuclei present, confinement can in addition significantly affect the crystallization kinetics of a polymer, often enhancing possible vitrification effects, which can be pronounced in organic semiconductors due to their complex chemical structure, as alluded to above.

Crystallization in confinement is, indeed, strongly influenced by nucleation. This can be exploited. For instance, by controlling the nucleation density and crystallization under confinement, a preferential orientation of the crystalline lamellae parallel to the π-stacking direction may be obtained. Results have furthermore shown that in P3HT the degree of chain orientation can increase with decreasing nucleation density (Figure 7a) and/or increase in confinement (Figure 7b). Thereby, the highest degree of orientation was achieved when the nucleation density matches the confinement area.[70]

The effect of confinement is often even more pronounced when using small-molecule semiconductors. This can be illustrated on p-DTS(FBTTh$_2$)$_2$ (see Figure 5 for its chemical structure), which has been shown to be highly sensitive to spatial confinement on device-relevant length scales.[71] By using as confining media electrochemically grown nanoporous anodic aluminum oxide (AAO) comprising nanopores of 25, 40, 60, 180, and 400 nm in diameter, with a 100 μm pore length, it was demonstrated that spatial confinement is an efficient tool to direct the crystal orientation and overall texture of this small molecule semiconductor in a controlled manner. More specifically, clear signs of spatial confinement were observed in differential scanning calorimetry.[71]

Yet, to consider the differences in the phase behavior of bulk samples versus thin films, it is important to note that these confinement effects only occur when the volume in which the material is solidified is very limited, like in ultrathin films or nanopores. For instance, for p-DTS(FBTTh$_2$)$_2$ confined in nanoporous structures discussed above, drastically reduced melting temperatures and new phase transitions were observed only when using pores of a diameter of 60 nm or less.[71] Indication for confinement affecting solidification can also be obtained from the observation that the crystallization temperature, T_c, strongly decreases with decreasing confinement pore diameter (up to a difference of 50 °C), exemplifying that a significant supercooling is needed to induce crystallization in confinement.[71] This suggests that *bulk* p-DTS(FBTTh$_2$)$_2$, like most organic matter, crystallizes from heterogeneities (impurities) that are present in the melt. Vice versa, in highly confined scenarios, the material will crystallize via a heterogeneity-free nucleation mechanism, such as homogeneous nucleation.[71] In this context, we like to highlight that, for example, F-DSC enables the measurement of thin to ultrathin films, thus overcoming the issue of some other methods that are limited to characterize only thick films while thin films are used in devices. In fact, F-DSC allows for the establishment of the thermal phase behavior of identical structures with respect to thickness as those used in devices.[39]

Combining the DSC data with information from X-ray diffraction, moreover, temperature/confinement phase diagrams can be established. Examples of cooling and heating diagrams for p-DTS(FBTTh$_2$)$_2$ confined in nanopores are displayed in Figure 8 which summarizes the rich phase behavior of this semiconducting small molecule as a function of both temperature and degree of spatial restriction (quantified in terms of inverse nanopore diameter).[71] The glass transition temperature, T_g, is also included.

Revealingly, such phase diagrams can be used to select different scenarios to solidify organic semiconductors; for p-DTS(FBTTh$_2$)$_2$ indicated as pathways I, II, and III in Figure 8.

https://doi.org/10.1021/acs.macromol.1c00296
Macromolecules 2021, 54, 5304−5320

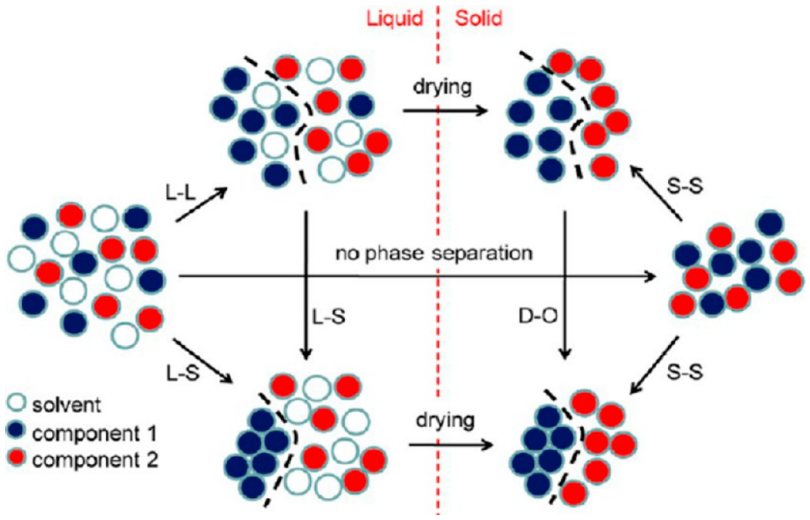

Figure 9. Schematic overview of the solidification processes that may occur during drying of a solution that contains a solvent and two solutes, as commonly used in the organic electronics field to prepare devices. Depending on the thermodynamic interactions between the two solutes, and the solutes and the solvent, as well as the solidification kinetics, liquid−liquid (L−L) demixing, liquid−solid (L−S) demixing, or vitrification can occur. Once in the solid state, a vitrified structure can phase separate via binodal decomposition or via crystallization of at least one component. Adapted from ref 72.

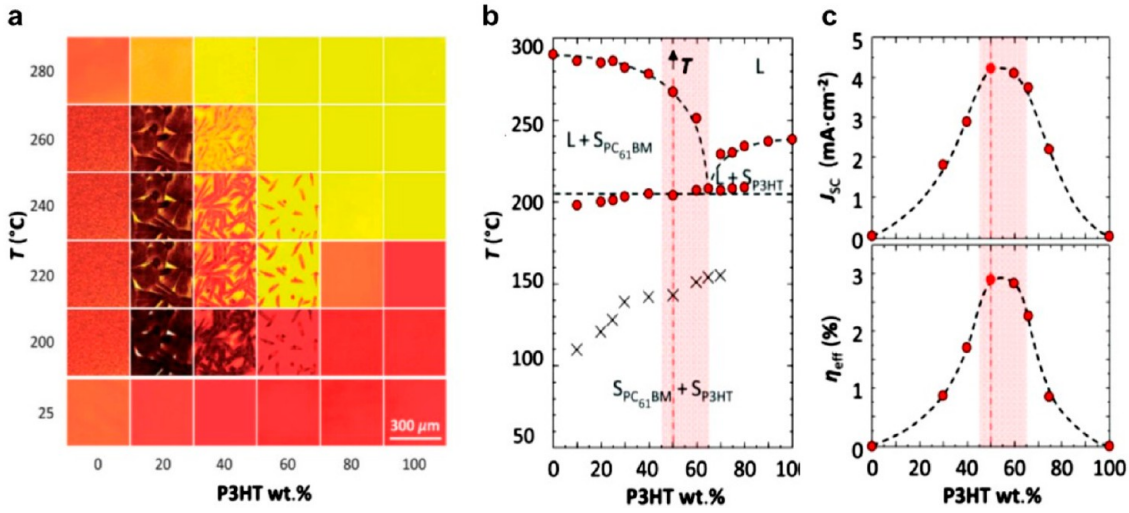

Figure 10. (a) Transmission optical micrographs of solution-cast P3HT:PCBM-C_{61} films for organic solar cell fabrication, taken during heating from an initially vitrified state (25 °C), illustrating the cold crystallization of the fullerene, followed by solid−solid phase separation. The crystals that form are PCBM-C_{61} primary crystals, only forming at P3HT fractions below 65 wt %. Melting of the P3HT can be inferred from the characteristic red to yellow transition observed by eye, indicating that its melting point is depressed upon addition of the fullerene, as often observed when a small molecule is added to a polymer. (b, c) Correlation of organic photovoltaic performance (after thermal annealing at 140 °C) and phase behavior of P3HT:PCBM-C_{61} blends. The nonequilibrium temperature/composition diagram in (b) was constructed from first heating thermograms of solution-cast material, revealing a eutectic behavior with the eutectic temperature occurring at 205 °C and a eutectic composition at 65 wt % of P3HT. Liquidus lines were constructed with end of melting and end of dissolution temperatures. Crosses represent the onset of recrystallization while highlighted areas indicate the range of compositions leading to optimum photovoltaic performance given in (c) with the short-circuit current (J_{sc}) and the overall device efficiency (η_{eff}). Adapted from ref 73.

Pathway I corresponds to the crystallization of *bulk* p-DTS(FBTTh$_2$)$_2$, pathway II to crystallization inside 400 nm diameter pores (i.e., at weak confinement), and pathway III to crystallization inside 40 nm diameter pores (i.e., at pronounced confinement). Depending on the pathway selected, different crystal textures can be induced in a highly controlled fashion, which was exploited for the manipulation of properties including photoluminescence and charge transport characteristics.[71]

TEMPERATURE/COMPOSITION PHASE DIAGRAMS

The phenomena and processes discussed in the previous sections often become more complicated when studying multicomponent systems/blends, common in many organic electronics and photonics applications. The reason is that liquid−liquid (L−L), solid−liquid (S−L), or solid−solid (S−S) demixing processes as well as disorder−order (D−O) transitions may compete with each other[72] as illustrated in the schematic presented in Figure 9, with significant impact on

https://doi.org/10.1021/acs.macromol.1c00296
Macromolecules 2021, 54, 5304−5320

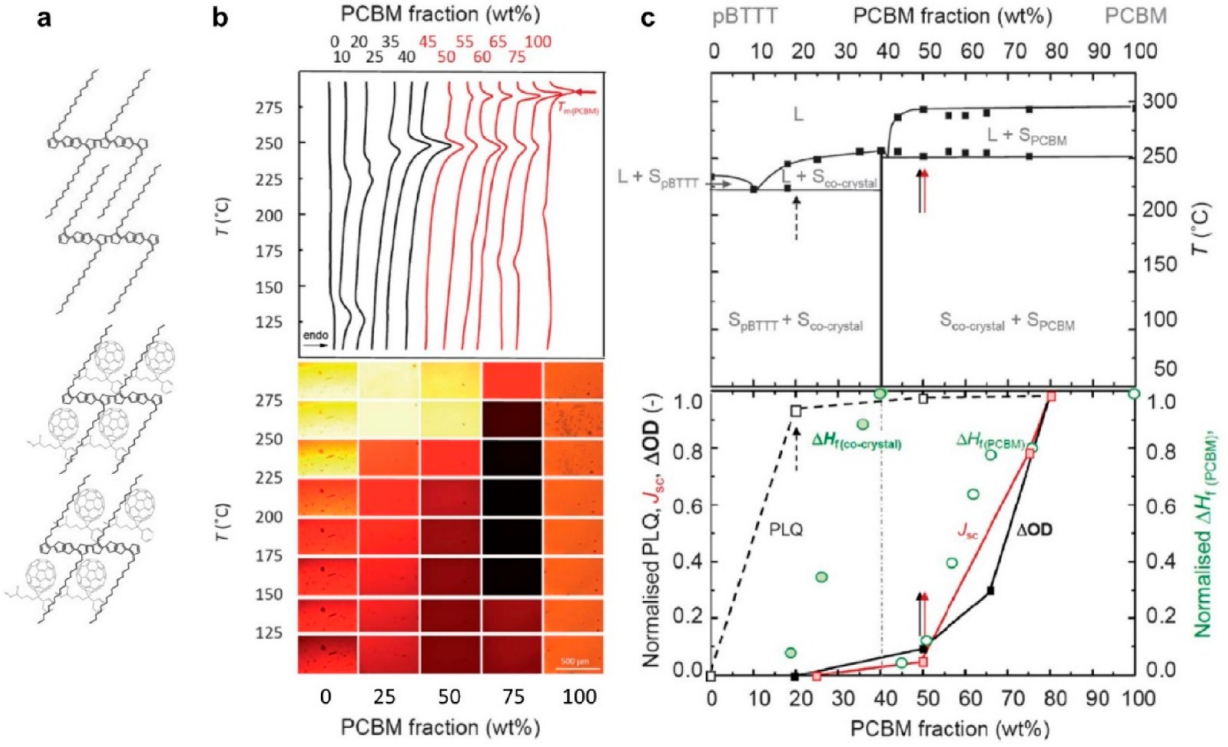

Figure 11. (a) Schematic representation of poly(2,5-bis(3-alkylthiophen-2-yl)thieno[3,2-*b*]thiophene), PBTTT, solid-state arrangement (top) and the one of its blends with fullerenes, where cocrystalline regions form with the fullerene intercalated within the PBTTT side chains (bottom). (b) Top: differential scanning calorimetry first heating thermograms of PBTTT:PCBM binaries. The endotherm at 280 °C is attributed to melting of crystalline PCBM domains. Bottom: transmission optical micrographs of solution-cast PBTTT:PCBM films which were then heated to different temperatures at a rate of 10 °C min^{-1}. Melting of the PBTTT:PCBM cocrystal as well as neat PBTTT can be inferred from the characteristic red to yellow transition observed at elevated temperatures, in good agreement with the thermal analysis data presented on top. For compositions of 75 wt % PCBM, the blend films crystallize upon heating above 150 °C (see exotherm observed in corresponding heating thermogram presented on top), which leads to a distinct darkening of these architectures. (c) Experimentally established nonequilibrium temperature/composition phase diagrams for PBTTT:PCBM-C_{61} constructed from the DSC and optical microscopy data presented in (b). While more complex, it can be identified that a single cocrystal phase forms at 40 wt % fullerene content. At higher or lower fullerene fractions, either PBTTT-rich domains coexist with cocrystalline regions or cocrystal domains coexist with fullerene-rich domains. This has direct consequence on the blend's optoelectronic performance. Indeed, based on the temperature/composition diagram plotted from the DSC and optical microscopy data (b), detailed property mapping can be achieved with respect to composition and temperature sets. Indeed, clear relations can, for instance, be established between short-circuit current, J_{sc}, charge generation (given here via the ΔOD obtained from transient absorption spectroscopy), and photoluminescence quenching, PLQ. The highest charge generation and J_{sc} are observed where fullerene-rich domains start to develop (indicated as S_{PCBM}) while highest PLQ is observed in areas where cocrystal formation dominates. Adapted from ref 86.

solid-state structure formation of blends such as those in organic photovoltaic device layers.[73−75]

Because all these processes, including liquid−liquid, liquid−solid, and solid−solid demixing, are temperature- and composition-dependent, temperature/composition phase diagrams can provide highly useful insights into the structure development of such multicomponent systems. Because they are constructed from experiments, usually they reflect a nonequilibrium scenario.

In a most simple manner, temperature/composition phase diagrams for polymer semiconductors can be established via optical microscopy,[73] as the example of the P3HT:PCBM-C_{61} binary in Figure 10a illustrates. This is because for many semiconducting macromolecules, and especially semiflexible materials such as P3HT, the solid-to-liquid melting transition can be followed visually via a color change induced by the polymer chains coiling up more strongly in the liquid phase, reducing the conjugation length and, thus, in the case of P3HT, leading to a transition from red to yellow appearance (Figure 10a).

Using this color change, it can be observed that addition of the fullerene at small fractions to the P3HT results in a reduction of the P3HT melting temperature. This effect seems to level off around 200 °C at P3HT concentrations of 65 wt % and below. Simultaneously, at these P3HT fractions (i.e., 20, 40, and 60 wt % P3HT), the formation of fullerene crystals can be found upon heating above 200 °C. These crystals gradually melt at different temperatures depending on the blend composition, with more PCBM-C_{61}-rich blends featuring crystals that melt at higher temperatures.[73]

These observations indicate a eutectic phase behavior,[63,76−78] which is formed by two solids that are typically immiscible in the solid state over a specific composition range, while being fully miscible at all compositions in the liquid phase. This leads at temperatures below 205 °C to temperature/composition regions where two solids coexist (here, a P3HT-rich phase and a fullerene-rich phase, at temperature around room temperature), while at higher temperatures (above 205 °C) either liquid P3HT exists with solid PCBM-C_{61} (i.e., the fullerene crystals clearly observed in optical microscopy) or liquid PCBM-C_{61} coexists with solid P3HT (at

https://doi.org/10.1021/acs.macromol.1c00296
Macromolecules 2021, 54, 5304−5320

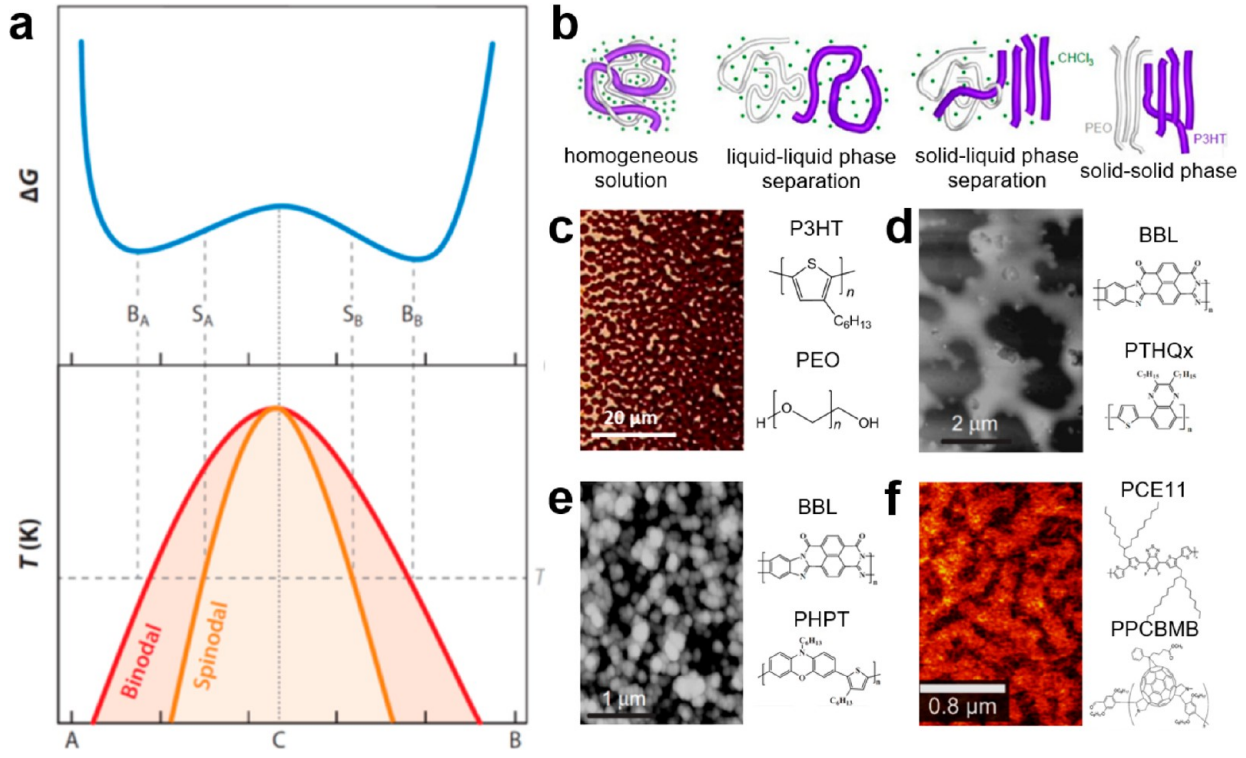

Figure 12. (a) Energy−temperature−composition diagram of a partially miscible binary polymer:polymer system undergoing LL phase separation. The Gibbs free energy, ΔG, at a given temperature, T, is plotted against composition. The phase boundaries between the one-phase to the two-phase regions, including the binodal and spinodal regions, are highlighted. (b) Schematics of the liquid−liquid phase separation process using as an example a blend between P3HT and poly(ethylene oxide) (PEO) in chloroform. (c) Optical micrograph of a phase-separated P3HT:PEO film after solvent evaporation. (d, e) AFM topographic images of phase-separated BBL:PTHQx (2:98 wt %) (d) and BBL:PHPT (20:80 wt %) (e). (f) AFM topographic image of a phase-separated PCE11:PPCBMB (50:50 wt %) thin film deposited by employing convective self-assembly. The chemical structures of blend components are shown in the insets (c−f). Adapted from ref 13 (a−c), ref 88 (d, e), and ref 89 (f).

P3HT fractions above 65 wt %). At even more elevated temperatures, above the liquidus lines, a fully miscible liquid phase is formed.[73]

Because both the addition of the polymer to the fullerene, and vice versa the introduction of the fullerene to the P3HT, lowers the melting point of the other component, typical for a eutectic phase behavior, a composition can be identified around 65 wt %, where the lowest melting point in the systems occurs (that is, the lowest T_m among all blend compositions). This composition is called the eutectic composition while the temperature at which a blend of the eutectic composition melts is called the eutectic temperature (≈205 °C). This behavior can more quantitatively be followed with differential scanning calorimetry, leading to a temperature/composition phase diagram as displayed in Figure 10b.

Most importantly, in direct analogy to metallurgy, temperature/composition phase diagrams can directly be related to specific blend properties (Figure 10c). For instance, in the case of the P3HT:PCBM-C_{61} binary, a direct correlation of temperature, composition, and photocurrent generation in photovoltaic cells can be made.[73] Specifically, as-prepared devices display a maximum short-circuit photocurrent, J_{sc}, at P3HT fractions close to the eutectic composition (Figure 10c). After thermal treatment at 140 °C for 45 min, a temperature within the range where cold-crystallization endotherms are observed in DSC (indicated with crosses in the phase diagram in Figure 10b), the short-circuit photocurrent can be maximized for blend films comprising 50−60 wt % P3HT, that is, at compositions within a slightly hypoeutectic regime. This observation can be explained as in the following: Given that exciton dissociation and charge separation occur at donor−acceptor interfaces, one requirement for efficient photocurrent generation is the maximization of the donor−acceptor solid−solid contact area.[79−83] This is likely achieved for blends of exactly the eutectic composition, where it is known from metallurgy that a very finely phase-separated microstructure develops.[76−78] However, high photocurrent additionally requires the existence of percolating, conductive pathways for the collection of both electrons and holes. Such a morophology is achieved in blends in which primary fullerene crystals form, enabling a charge-transport pathway for electrons through the bulk of the film while the polymeric donor naturally forms a network by the very virtue of its entangled, macromolecular nature.[84]

Temperature/composition phase diagrams can also be highly useful in blend systems where, for example, the polymer semiconductor can cocrystallize with the other active component. This can lead to well-defined single-phase "cocrystalline" domains (i.e., solid solutions) composed of molecules of both blend components (see Figure 11a for schematics of the structural arrangement of neat PBTTT and polymer:fullerene cocrystalline assemblies).[85] A most illustrative example of binary blends experiencing cocrystallization is given by the PBTTT:PCBM-C_{61} system[86]—another donor:acceptor blend used in organic photovoltaics. In this case, the rather complex phase behavior, as determined by thermal analysis and optical microscopy (Figure 11b), is dictated by PBTTT-rich and PCBM-C_{61}-rich phases as well as

https://doi.org/10.1021/acs.macromol.1c00296
Macromolecules 2021, 54, 5304−5320

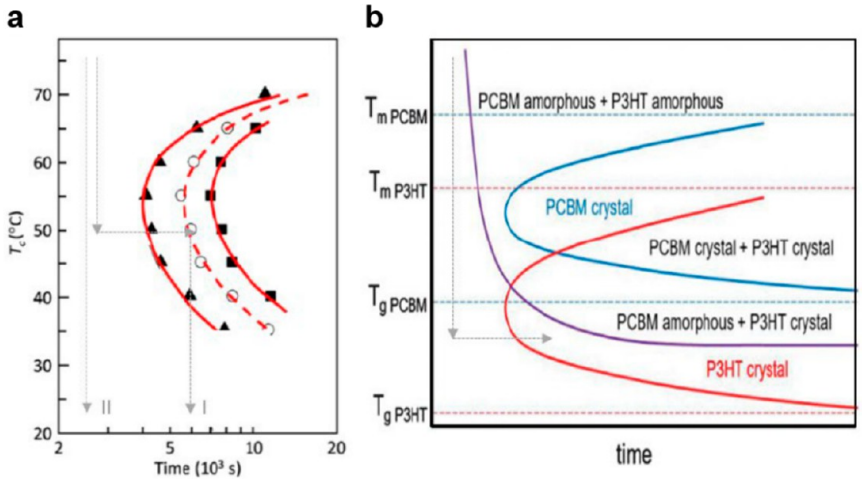

Figure 13. Illustrative examples of a few functional polymer time/temperature/transformation (TTT) in the literature.[90,91] (a) TTT phase diagram deduced for poly(3-(2′-ethyl)hexylthiophene) (P3EHT) from DSC heating scans that give the time of the onset of crystallization (triangles). The time after full crystallization (10 J/g: squares) and the time needed to go halfway through the transformation (i.e., after an enthalpy of 5 J/g is reached; circles) are also indicated. Solidification pathways that lead to a sample of 50% maximum reachable crystallinity (I) vs fully vitrified samples (II) can be identified. (b) Hypothetical TTT "Gedanken experiment" for a solar cell blend (P3HT and the fullerene PCBM), displaying the competing processes of spinodal decompositions (purple), PCBM crystallization (blue), and P3HT crystallization (red). If the material is first quenched and then solidified, P3HT crystallization can occur. Adapted from ref 95 (a) and ref 96 (b).

a "cocrystal" phase formed by the two via intercalation of the fullerene within the PBTTT side chains. This system leads to two eutectics: one formed at low fullerene contents between PBTTT and the cocrystalline PBTTT:PCBM-C_{61} structures and another one formed at high PCBB-C_{61} fractions between PBTTT:PCBM-C_{61} "cocrystals" and the fullerene (Figure 11c).[86]

Direct correlations and property mapping with temperature and compositions can again be made. Blends comprising high amounts of cocrystalline regions experience higher photoluminescence quenching of the polymer, in agreement with the general view that polymer exciton quenching occurs within molecularly mixed phases. It is also apparent that both short-circuit photocurrent, J_{sc}, and the dissociated polaron yield (ΔOD), which gives insight into charge generation, rapidly increase once the fullerene content exceeds the eutectic composition of the cocrystal:PCBM-C_{61} binary (≈44 wt % PCBM-C_{61}), that is, at compositions where relatively phase-pure primary fullerene crystals start to develop, similar to the P3HT:PCBM-C_{61} binary.[86]

Blends can also be made of two or more conjugated polymers. Such blends typically exhibit only partial miscibility and, thus, tend to undergo liquid−liquid (LL) phase separation. For example, during cooling, phase separation proceeds via spinodal or binodal decomposition into amorphous regions[18] or by crystallization and aggregation. When crystallization does not dominate, polymer:polymer blends display in most cases an upper critical solution temperature (UCST),[18] where a single phase is only formed at elevated temperatures and in a region outside the binodal line (Figure 12a).[13] At temperatures above the UCST, binaries typically exhibit a single energetic minimum as a function of composition and temperature, thus favoring the formation of a single phase. Below the UCST the free energy landscape may exhibit two local minima and thus pushes the system to phase separate.[13] The difference between spinodal and binodal decomposition can be better understood when plotting a Gibbs free energy curve (Figure 12a). At a given temperature T_x, in the spinodal region, the curvature of the free energy as a function of composition is negative, and thus, a spontaneous phase separation of the two components can occur (Figure 12b,c). The binodal region located between the spinodal curve and the two energetic minima exhibits a positive curvature of the free energy, and thus, metastable blend compositions can form. Such blends can be rapidly "quenched" into a single-phase system, although over time and/or at elevated temperatures, they will eventually reach the equilibrium phase-separated state.[13]

A recent example of conjugated binary polymer:polymer blends is given by the mixture of polyfluorene derivatives with alternating thiophene-/benzothiadiazole-containing copolymers.[87] Such blends, exhibiting a "hydrodynamically" trapped miscible state (i.e., a dynamic miscibility induced through the use of external mechanical stimuli), were shown to undergo a distinct phase separation with self-restorable fluorescence color changes.[87] In addition, the phase separation of blends composed of poly(benzobisimidazobenzophenanthroline) (BBL) and poly[(thiophene-2,5-diyl)-*alt*-(2,3-diheptyl-quinoxaline-5,8-diyl)] (PTHQx) as well as poly(10-hexylphenoxazine-3,7-diyl-*alt*-3-hexyl-2,5-thiophene) (PHPT), i.e., blends comprising an electron and a hole conductor, was used to alter the final charge transport properties of such multicomponent systems. It was shown that phase-separated BBL:PTHQx and BBL:PHPT blends (Figure 12d,e) displayed a high electron mobility and favored ambipolar charge transport at high fractions of the hole-conducting polymer.[88] Other examples of binary polymer:polymer blends, where phase separation was exploited to manipulate the systems' optoelectronic properties, are binary systems of the electron-donating poly[(5,6-difluoro-2,1,3-benzothiadiazol-4,7-diyl)-*alt*-(3,3′-di(2-octyldodecyl)2,2′;5′,2′;5′,2′-quaterthiophen-5,5′-diyl)] (PCE11) and poly[[bispyrrolidino(phenyl-C_{61}-butyric acid methyl ester)]-*alt*-[2,5-bis(octyloxy)benzene]] (PPCBMB) (Figure 12f)[89] as well as blends of the electron-accepting poly(2,2′-(3,3-dioctyl-2,2′-bithienylene)-6,6′-bis(4-phenylenequinoline)) (POBTPQ) and the electron-donating

https://doi.org/10.1021/acs.macromol.1c00296
Macromolecules 2021, 54, 5304−5320

poly(3-octylthiophene) (POT) and poly(2-methoxy-5-(2′-ethylhexyloxy)-1,4-phenylenevinylene) (MEH-PPV).[90] [Note: similar considerations, of course, apply to blocky copolymers, including diblock copolymers. This was shown, for example, for materials with two flexible blocks, that is, a P3HT and a polyethylene block, which were shown to microphase-separate leading to thin-film structures of essentially identical charge-transport properties as found in P3HT, but with improved on–off ratios (as measured in thin-film transistors) and notably enhanced mechanical properties, as deduced from measured elongations at break exceeding 600% and true tensile strengths around 70 MPa).[91]]

TIME/TEMPERATURE/TRANSFORMATION PHASE DIAGRAMS

Our discussion concludes with time/temperature/transformation (TTT) diagrams, also called isothermal transformation diagrams, which are unique tools that can provide a window into the detailed temporal and dynamic progression of the solid-state development of materials. As a function of a given material's composition, TTT diagrams provide comprehensive insights not only into the type of phase transformations a material system undergoes but also details on the time it takes for a transition to complete at a given temperature and the stability of specific phases under, for example, isothermal transformation conditions. Despite this great promise and their broad use in establishing processing guidelines for metal alloys, TTT phase diagrams unfortunately have rarely been utilized in the field of functional polymers.[92−94] More common use of TTT phase diagrams in the broader polymer community could enable the field to understand the kinetics and mechanisms of functional polymer thin film growth (and production of other architectures) contributing to a transformation in manufacturing of organic electronics/photonics products and beyond.

An illustration of the utility of TTT phase diagrams is given with the example of poly(3-(2′-ethyl)hexylthiophene) (P3EHT).[95] The TTT phase diagram for this polymer semiconductor displays a typical C-shape for onset and end of crystallization (Figure 13a). The earliest onset of crystallization occurs during isothermal solidification at 55 °C. At higher temperatures, nucleation is limited and, hence, the crystallization onset is delayed. In contrast, at lower temperatures diffusive transport becomes slower, thus limiting the crystallization rate despite the increased number of nucleation sites. Accordingly, immediate information is obtained with respect to temperatures that need to be selected to control crystal size (low vs high number of nuclei) and, for example, annealing times at specific temperatures. Indeed, from TTT diagrams, one can extract the time needed to reach maximum degree of crystallinity at given isothermal conditions or a certain percentage of the maximum achievable crystallinity. For instance, in the case of P3EHT kept for 6000 s at 55 °C, half of the maximum degree of crystallinity achievable in this material can be obtained (pathway I in Figure 13a), while when quenched rapidly, a fully amorphous material is induced (pathway II), which will slowly crystallize over time. This information can be readily used to understand certain aging processes or to develop processing protocols by predicting isothermal solidification times necessary to obtain a structure of a specific crystalline content.

TTT diagrams can further be used to decipher the phase behavior of various blend systems. One hypothetical diagram was, for example, drawn for the P3HT:PCBM-C_{61} binary (Figure 13b),[96] which illustrates the competition between processes, such as liquid–liquid demixing, crystallization of either the fullerene or the polymer, and vitrification. It highlights that rapid cooling leads to a strongly vitrified blend (indicated in Figure 13b with gray arrows); held above the glass transition temperature of P3HT but below that of PCBM-C_{61}, crystallization of the polymer may occur. In contrast, structure formation is dominated by spinodal decomposition at more elevated temperatures.

The establishment of TTT phase diagrams for polymer blends, especially when processed from solution, can be challenging; this perhaps explains their scarcity in the literature. A simpler alternative can be to construct the temperature/composition phase diagrams for each component with the common solvent and superimposing these. Such quasi-binary phase diagrams provide essential information with respect to which process sets in first when selecting a specific solidification pathway. An exemplary quasi-binary temperature/composition phase diagram, which can deliver some of the information TTT phase diagrams provide, is displayed in Figure 14 for the ternary P3HT, polyethylene (PE), and

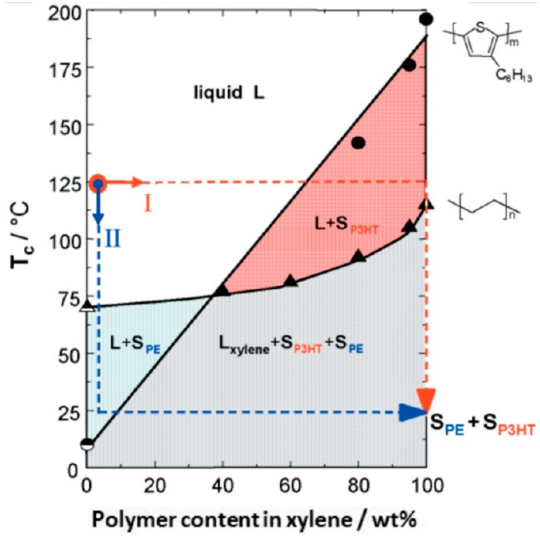

Figure 14. Crystallization temperature/composition diagram for P3HT:PE blends constructed with peak crystallization temperatures of either P3HT or PE in xylene, determined by differential scanning calorimetry, except for highly dilute solutions.[92] The different phases are indicated: Liquid, L; solid P3HT, S_{P3HT}; and solid PE, S_{PE}. Depending on the solidification pathway (I: hot-casting above the crystallization temperature of PE leading the P3HT to crystallize first; II: room temperature casting resulting in the PE to solidify prior to P3HT), very different solid-state structures and, hence, macroscopic properties, such as charge transport, are induced. Adapted from ref 97.

xylene,[97] established from the crystallization temperatures of P3HT in xylene and of PE in xylene, recorded with differential scanning calorimetry, and then superimposed. It shows that the crystallization sequence of the two solutes can be controlled via selection of the casting temperature/conditions. When, for instance, the P3HT:PE:xylene solution is deposited at elevated temperatures above the crystallization temperature of neat PE (pathway I in Figure 14), initially, the solvent starts to evaporate. The solution concentrates, and the semiconductor crystallizes once sufficient solvent is evaporated, all while the polyethylene stays molten. Further cooling of this binary to room temperature will induce subsequent crystallization of PE

https://doi.org/10.1021/acs.macromol.1c00296
Macromolecules 2021, 54, 5304−5320

from a melt condition. Because of the strong driving force of linear polyethylene to crystallize, even in the blend and in the presence of the solidified P3HT, the insulator molecularly orders, resulting in a double-percolating P3HT structure leading to excellent charge transport both in field-effect transistors and in the bulk.[97,99] Intriguingly, the addition of the polyethylene also has a stabilizing effect on important device characteristics such as bias stress and shelf lifetime.[98] In strong contrast, when the blend is cast at room temperature from a hot xylene solution, the solution rapidly cools, resulting in the PE crystallizing first around 73 °C for a dilute solution, while the P3HT only solidifies once the solvent starts to evaporate. Accordingly, solid-state structure formation is dictated by the PE crystallization, hindering the semiconductor to molecularly order and leading to architectures of very poor charge transport. These insights are rather universally applicable, for instance, to blends of PE with polymeric electron conductors as well as ternaries for solar cell applications, including P3HT:PCBM-C_{61}:PE blends.[100]

CONCLUSIONS

Recent advances connecting phenomena during the solidification and solid-state structure development of conjugated polymers have led to important insights into how to manipulate properties such as light emission, charge transport, and charge generation in a controlled fashion. Common approaches in other fields of materials science, such as the establishment and use of temperature/composition, temperature/confinement, and time/temperature/transformation diagrams, may thereby open new opportunities toward a predictive knowledge platform for assembly of single- and multicomponent polymer semiconductors. We, thus, expect that the more frequent incorporation of these approaches and tools will lead to a step change in how structure−property relationships are unveiled in these promising materials systems and how new pathways are opened toward new materials systems and novel device architectures.

AUTHOR INFORMATION

Corresponding Author

Natalie Stingelin − *School of Chemical and Biochemical Engineering and School of Materials Science and Engineering, Georgia Institute of Technology, Atlanta, Georgia 30332-0245, United States;* orcid.org/0000-0002-1414-4545; Email: natalie.stingelin@mse.gatech.edu

Authors

Ioan Botiz − *Interdisciplinary Research Institute on Bio-Nano-Sciences, Babes-Bolyai University, Cluj-Napoca 400271, Romania*

Marlow M. Durbin − *School of Chemical and Biochemical Engineering, Georgia Institute of Technology, Atlanta, Georgia 30332-0245, United States*

Complete contact information is available at: https://pubs.acs.org/10.1021/acs.macromol.1c00296

Funding

I.B. acknowledges funding by the Romanian National Authority for Scientific Research and Innovation, CNCS−UEFISCDI, Project PN-III-P2-2.1-PED-2019-3995. M.M.D. is grateful for support via a National Science Foundation (NSF) Graduate Research Fellowship under Grant DGE-1650044, and N.S. thanks the NSF for the funded DMR Project 1905901.

Notes

The authors declare no competing financial interest.

Biographies

Dr. Habil. Ioan Botiz was a Marie Curie fellow at the French National Centre for Scientific Research and received, in 2007, his PhD in polymer physics from the Haute Alsace University. He then moved to Center for Nanoscale Materials at Argonne National Laboratory and focused on structuring of photovoltaic active layers and fabrication of organic energy devices. Ioan returned to Europe as a FRIAS excellence postdoctoral fellow at the University of Freiburg where he was working to understand the structure−property relationships in conjugated polymers. Since 2014, he has been working at Babes-Bolyai University where he holds the position of Scientific Researcher 1. He was also a Research Associate at Imperial College London (2014−2019).

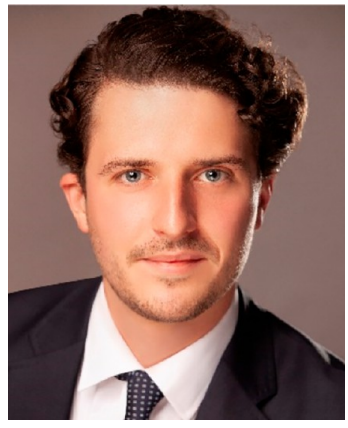

Marlow M. Durbin was born in Chicago, IL, and received his B.S. in Chemical & Biological Engineering from the University of Alabama in 2018. While at Alabama, he did undergraduate research with Prof. Jason Bara characterizing ionic polyimides and their blends with room temperature ionic liquids (IL's) for gas separations and additive manufacturing. Marlow is currently working towards his PhD in Chemical & Biomolecular Engineering under the supervision of Professor Natalie Stingelin at the Georgia Institute of Technology, supported by an NSF Graduate Research Fellowship. His research centers on processing and characterization of mixed ionic−electronic conducting blends and inorganic/organic hybrid materials for bioelectronics applications.

https://doi.org/10.1021/acs.macromol.1c00296
Macromolecules 2021, 54, 5304−5320

Natalie Stingelin is a Full Professor at the Georgia Institute of Technology with a joint appointment at the School of Materials Science & Engineering and the School of Chemical & Biomolecular Engineering, with prior positions at Imperial College London, UK; at Queen Mary University of London, UK; the Philips Research Laboratories in Eindhoven, The Netherlands; the Cavendish Laboratories, University of Cambridge, UK; and the Swiss Federal Institute of Technology (ETH) Zürich, Switzerland. She is the Co-Director of Georgia Tech's Center of Organic Electronics and Photonics and holds a Chaire Internationale Associée by the Excellence Initiative of the Université de Bordeaux since 2017. Natalie was elected a 2019 Fellow of the Materials Research Society and has been a Fellow of the Royal Society of Chemistry since 2012.

REFERENCES

(1) Yamamoto, T.; Shimizu, T. New π-conjugated polymers containing tetrathiafulvalene as the monomeric unit. *J. Mater. Chem.* **1997**, *7*, 1967−1968.

(2) Moigne, J. L.; Soldera, A.; Guillon, D.; Skoulios, A. Acetylenic and diacetylenic liquid-crystalline monomers: towards ordered conjugated polymers. *Liq. Cryst.* **1989**, *6*, 627−639.

(3) Keller, A. A note on single crystals in polymers: Evidence for a folded chain configuration. *Philos. Mag.* **1957**, *2*, 1171−1175.

(4) de Gennes, P.-G. *Scaling Concepts in Polymer Physics*; Cornell University Press: Ithaca, NY, 1979.

(5) Doi, M.; Edwards, S. F. *The Theory of Polymer Dynamics*; Clarenderon Press: Oxford, 1986.

(6) Sommerville, P. J. W.; Li, Y.; Dong, B. X.; Zhang, Y.; Onorato, J. W.; Tatum, W. K.; Balzer, A. H.; Stingelin, N.; Patel, S. N.; Nealey, P. F.; Luscombe, C. K. Elucidating the Influence of Side-Chain Circular Distribution on the Crack Onset Strain and Hole Mobility of Near-Amorphous Indacenodithiophene Copolymers. *Macromolecules* **2020**, *53*, 7511−7518.

(7) Koch, F. P. V.; Rivnay, J.; Foster, S.; Müller, C.; Downing, J. M.; Buchaca-Domingo, E.; Westacott, P.; Yu, L.; Yuan, M.; Baklar, M.; Fei, Z.; Luscombe, C.; McLachlan, M. A.; Heeney, M.; Rumbles, G.; Silva, C.; Salleo, A.; Nelson, J.; Smith, P.; Stingelin, N. The impact of molecular weight on microstructure and charge transport in semicrystalline polymer semiconductors−poly(3-hexylthiophene), a model study. *Prog. Polym. Sci.* **2013**, *38*, 1978−1989.

(8) Hallam, T.; Lee, M.; Zhao, N.; Nandhakumar, I.; Kemerink, M.; Heeney, M.; McCulloch, I.; Sirringhaus, H. Local Charge Trapping in Conjugated Polymers Resolved by Scanning Kelvin Probe Microscopy. *Phys. Rev. Lett.* **2009**, *103*, 256803.

(9) McCulloch, I.; Heeney, M.; Bailey, C.; Genevicius, K.; MacDonald, I.; Shkunov, M.; Sparrowe, D.; Tierney, S.; Wagner, R.; Zhang, W.; Chabinyc, M. L.; Kline, R. J.; McGehee, M. D.; Toney, M. F. Liquid-crystalline semiconducting polymers with high charge-carrier mobility. *Nat. Mater.* **2006**, *5*, 328−333.

(10) Heeney, M.; Bailey, C.; Genevicius, K.; Shkunov, M.; Sparrowe, D.; Tierney, S.; McCulloch, I. Stable Polythiophene Semiconductors Incorporating Thieno[2,3-b]thiophene. *J. Am. Chem. Soc.* **2005**, *127*, 1078−1079.

(11) Reid, O. G.; Malik, J. A. N.; Latini, G.; Dayal, S.; Kopidakis, N.; Silva, C.; Stingelin, N.; Rumbles, G. The influence of solid-state microstructure on the origin and yield of long-lived photogenerated charge in neat semiconducting polymers. *J. Polym. Sci., Part B: Polym. Phys.* **2012**, *50*, 27−37.

(12) Wunderlich, B. *Macromolecular Physics*; Academic Press: New York, 1976; Vol. *2*.

(13) Stingelin, N. Establishing the thermal phase behavior and its influence on optoelectronic properties of semiconducting polymers. In *Conjugated Polymers: Properties, Processing, and Applications*; Reynolds, J. R., Thompson, B. C., Skotheim, T. A., Eds.; CRC Press: Boca Raton, FL, 2019.

(14) Gibbs, J. W.; Bumstead, H. A.; Name, R. G. V.; Longley, W. R. *The Collected Works of J. Willard Gibbs*; Longmans, Green & Co.: Madison, WI, 1902.

(15) Thomson, J. J. *Applications of Dynamics to Physics and Chemistry*; Adamant Media: Boston, MA, 2005.

(16) Flory, P. J.; Yoon, D. Y. Molecular morphology in semicrystalline polymers. *Nature* **1978**, *272*, 226−229.

(17) Keller, A. Polymer crystals. *Rep. Prog. Phys.* **1968**, *31*, 623−704.

(18) Treat, N. D.; Westacott, P.; Stingelin, N. The Power of Materials Science Tools for Gaining Insights into Organic Semiconductors. *Annu. Rev. Mater. Res.* **2015**, *45*, 459−490.

(19) Rahimi, K.; Botiz, I.; Stingelin, N.; Kayunkid, N.; Sommer, M.; Koch, F. P. V.; Nguyen, H.; Coulembier, O.; Dubois, P.; Brinkmann, M.; Reiter, G. Controllable Processes for Generating Large Single Crystals of Poly(3-hexylthiophene). *Angew. Chem., Int. Ed.* **2012**, *51*, 11131−11135.

(20) Rahimi, K.; Botiz, I.; Agumba, J. O.; Motamen, S.; Stingelin, N.; Reiter, G. Light absorption of poly(3-hexylthiophene) single crystals. *RSC Adv.* **2014**, *4*, 11121−11123.

(21) Hourani, W.; Rahimi, K.; Botiz, I.; Koch, F.; Reiter, G.; Lienerth, P.; Heiser, T.; Bubendorff, J.-L.; Simon, L. Anisotropic Charge Transport in Large Single Crystals of Pi-conjugated Organic Molecules. *Nanoscale* **2014**, *6*, 4774−4780.

(22) Kohn, P.; Huettner, S.; Komber, H.; Senkovskyy, V.; Tkachov, R.; Kiriy, A.; Friend, R. H.; Steiner, U.; Huck, W. T. S.; Sommer, J.-U.; Sommer, M. On the role of single regiodefects and polydispersity in regioregular poly(3-hexylthiophene): defect distribution, synthesis of defect-free chains, and a simple model for the determination of crystallinity. *J. Am. Chem. Soc.* **2012**, *134*, 4790−4805.

(23) Grozev, N.; Botiz, I.; Reiter, G. Morphological instabilities of polymer crystals. *Eur. Phys. J. E: Soft Matter Biol. Phys.* **2008**, *27*, 63−71.

(24) Koch, F. P. V.; Heeney, M.; Smith, P. Thermal and Structural Characteristics of Oligo(3-hexylthiophene)s $(3HT)_n$, $n = 4 - 36$. *J. Am. Chem. Soc.* **2013**, *135*, 13699−13709.

(25) Virkar, A. A.; Mannsfeld, S.; Bao, Z.; Stingelin, N. Organic Semiconductor Growth and Morphology Considerations for Organic Thin-Film Transistors. *Adv. Mater.* **2010**, *22*, 3857−3875.

(26) Wunderlich, B. *Macromolecular Physics*; Academic Press: New York, 1973; Vol. *1*.

(27) Keller, A.; O'Connor, A. Study of single crystals and their associations in polymers. *Discuss. Faraday Soc.* **1958**, *25*, 114−121.

(28) Marsh, H. S.; Reid, O. G.; Barnes, G.; Heeney, M.; Stingelin, N.; Rumbles, G. Control of polythiophene film microstructure and charge carrier dynamics through crystallization temperature. *J. Polym. Sci., Part B: Polym. Phys.* **2014**, *52*, 700−707.

(29) Muller, C.; Zhigadlo, N. D.; Kumar, A.; Baklar, M. A.; Karpinski, J.; Smith, P.; Kreouzis, T.; Stingelin, N. Enhanced Charge-Carrier Mobility in High-Pressure-Crystallized Poly(3-hexylthiophene). *Macromolecules* **2011**, *44*, 1221−1225.

(30) Guha, S.; Chandrasekhar, M.; Scherf, U.; Knaapila, M. Tuning structural and optical properties of blue-emitting polymeric semiconductors. *Phys. Status Solidi B* **2011**, *248*, 1083−1090.

(31) Huang, Y.-S.; Gierschner, J.; Schmidtke, J. P.; Friend, R. H.; Beljonne, D. Tuning interchain and intrachain interactions in

https://doi.org/10.1021/acs.macromol.1c00296
Macromolecules 2021, 54, 5304−5320

polyfluorene copolymers. *Phys. Rev. B: Condens. Matter Mater. Phys.* **2011**, *84*, 205311.
(32) Chabinyc, M. L.; Toney, M. F.; Kline, R. J.; McCulloch, I.; Heeney, M. X-ray Scattering Study of Thin Films of Poly(2,5-bis(3-alkylthiophen-2-yl)thieno[3,2-b]thiophene). *J. Am. Chem. Soc.* **2007**, *129*, 3226−3237.
(33) DeLongchamp, D. M.; Kline, R. J.; Jung, Y.; Lin, E. K.; Fischer, D. A.; Gundlach, D. J.; Cotts, S. K.; Moad, A. J.; Richter, L. J.; Toney, M. F.; Heeney, M.; McCulloch, I. Molecular Basis of Mesophase Ordering in a Thiophene-Based Copolymer. *Macromolecules* **2008**, *41*, 5709−5715.
(34) Zhang, X.; Bronstein, H.; Kronemeijer, A. J.; Smith, J.; Kim, Y.; Kline, R. J.; Richter, L. J.; Anthopoulos, T. D.; Sirringhaus, H.; Song, K.; Heeney, M.; Zhang, W.; McCulloch, I.; DeLongchamp, D. M. Molecular origin of high field-effect mobility in an indacenodithiophene−benzothiadiazole copolymer. *Nat. Commun.* **2013**, *4*, 2238.
(35) Bronstein, H.; Leem, D. S.; Hamilton, R.; Woebkenberg, P.; King, S.; Zhang, W.; Ashraf, R. S.; Heeney, M.; Anthopoulos, T. D.; Mello, J. d.; McCulloch, I. Indacenodithiophene-co-benzothiadiazole Copolymers for High Performance Solar Cells or Transistors via Alkyl Chain Optimization. *Macromolecules* **2011**, *44*, 6649−6652.
(36) Snyder, C. R.; Delongchamp, D. M.; Nieuwendaal, R. C.; Herzig, A. A. Structure and Order in Organic Semiconductors. In *Polymer Chemistry Series No. 21, Semiconducting Polymers: Controlled Synthesis and Microstructure*; Luscombe, C., Ed.; Royal Society of Chemistry: Cambridge, UK, 2017; pp 219−274.
(37) Baklar, M. A.; Koch, F.; Kumar, A.; Buchaca Domingo, E.; Campoy-Quiles, M.; Feldman, K.; Yu, L.; Wobkenberg, P.; Ball, J.; Wilson, R. M.; McCulloch, I.; Kreouzis, T.; Heeney, M.; Anthopoulos, T.; Smith, P.; Stingelin, N. Solid-state processing of organic semiconductors. *Adv. Mater.* **2010**, *22*, 3942−3947.
(38) Martín, J.; Stingelin, N.; Cangialosi, D. Direct Calorimetric Observation of the Rigid Amorphous Fraction in a Semiconducting Polymer. *J. Phys. Chem. Lett.* **2018**, *9*, 990−995.
(39) Marina, S.; Kaufmann, N. P.; Karki, A.; Gutiérrez-Meza, E.; Gutiérrez-Fernández, E.; Vollbrecht, J.; Solano, E.; Walker, B.; Bannock, J. H.; de Mello, J.; Silva, C.; Nguyen, T.-Q.; Cangialosi, D.; Stingelin, N.; Martín, J. The Importance of Quantifying the Composition of the Amorphous Intermixed Phase in Organic Solar Cells. *Adv. Mater.* **2020**, *32*, 2005241.
(40) Olsen, B. D.; Jang, S.-Y.; Lüning, J. M.; Segalman, R. A. Higher Order Liquid Crystalline Structure in Low-Polydispersity DEH-PPV. *Macromolecules* **2006**, *39*, 4469−4479.
(41) Zhang, W.; Gomez, E. D.; Milner, S. T. Predicting Nematic Phases of Semiflexible Polymers. *Macromolecules* **2015**, *48*, 1454−1462.
(42) Greco, C.; Jiang, Y.; Chen, J. Z. Y.; Kremer, K.; Daoulas, K. C. Maier-Saupe model of polymer nematics: Comparing free energies calculated with Self Consistent Field theory and Monte Carlo simulations. *J. Chem. Phys.* **2016**, *145*, 184901.
(43) Ramírez-Hernández, A.; Hur, S.-M.; Armas-Pérez, J. C.; Cruz, M. O.; De Pablo, J. J. Demixing by a Nematic Mean Field: Coarse-Grained Simulations of Liquid Crystalline Polymers. *Polymers* **2017**, *9*, 88.
(44) Olsen, B. D.; Shah, M.; Ganesan, V.; Segalman, R. A. Universalization of the Phase Diagram for a Model Rod-Coil Diblock Copolymer. *Macromolecules* **2008**, *41*, 6809−6817.
(45) Daoulas, K. C.; Rühle, V.; Kremer, K. Simulations of nematic homopolymer melts using particle-based models with interactions expressed through collective variables. *J. Phys.: Condens. Matter* **2012**, *24*, 284121.
(46) Kipp, D.; Ganesan, V. Influence of Block Copolymer Compatibilizers on the Morphologies of Semiflexible Polymer/Solvent Blends. *J. Phys. Chem. B* **2014**, *118*, 4425−4441.
(47) Snyder, C. R.; Kline, R. J.; DeLongchamp, D. M.; Nieuwendaal, R. C.; Richter, L. J.; Heeney, M.; McCulloch, I. Classification of semiconducting polymeric mesophases to optimize device post-processing. *J. Polym. Sci., Part B: Polym. Phys.* **2015**, *53*, 1641−1653.
(48) Heeney, M.; Bailey, C.; Giles, M.; Shkunov, M.; Sparrowe, D.; Tierney, S.; Zhang, W.; McCulloch, I. Alkylidene Fluorene Liquid Crystalline Semiconducting Polymers for Organic Field Effect Transistor Devices. *Macromolecules* **2004**, *37*, 5250−5256.
(49) Bridges, C. R.; Ford, M. J.; Bazan, G. C.; Segalman, R. A. Molecular Considerations for Mesophase Interaction and Alignment of Lyotropic Liquid Crystalline Semiconducting Polymers. *ACS Macro Lett.* **2017**, *6*, 619−624.
(50) Pisula, W.; Zorn, M.; Chang, J. Y.; Müllen, K.; Zentel, R. Liquid Crystalline Ordering and Charge Transport in Semiconducting Materials. *Macromol. Rapid Commun.* **2009**, *30*, 1179−1202.
(51) Mathot, V.; Pyda, M.; Pijpers, T.; Vanden Poel, G.; van de Kerkhof, E.; van Herwaarden, S.; van Herwaarden, F.; Leenaers, A. The Flash DSC 1, a power compensation twin-type, chip-based fast scanning calorimeter (FSC): First findings on polymers. *Thermochim. Acta* **2011**, *522*, 36−45.
(52) Orava, J.; Greer, A. L.; Gholipour, B.; Hewak, D. W.; Smith, C. E. Characterization of supercooled liquid Ge2Sb2Te5 and its crystallization by ultrafast-heating calorimetry. *Nat. Mater.* **2012**, *11*, 279−283.
(53) Chen, M.; Du, M.; Jiang, J.; Li, D.; Jiang, W.; Zhuravlev, E.; Zhou, D.; Schick, C.; Xue, G. Verifying the symmetry of ultra-fast scanning calorimeters using liquid crystal secondary temperature standards. *Thermochim. Acta* **2011**, *526*, 58−64.
(54) Mileva, D.; Androsch, R. Effect of co-unit type in random propylene copolymers on the kinetics of mesophase formation and crystallization. *Colloid Polym. Sci.* **2012**, *290*, 465−471.
(55) Bosq, N.; Guigo, N.; Zhuravlev, E.; Sbirrazzuoli, N. Nonisothermal Crystallization of Polytetrafluoroethylene in a Wide Range of Cooling Rates. *J. Phys. Chem. B* **2013**, *117*, 3407−3415.
(56) Stolte, I.; Androsch, R.; Di Lorenzo, M. L.; Schick, C. Effect of Aging the Glass of Isotactic Polybutene-1 on Form II Nucleation and Cold Crystallization. *J. Phys. Chem. B* **2013**, *117*, 15196−15203.
(57) Mollova, A.; Androsch, R.; Mileva, D.; Schick, C.; Benhamida, A. Effect of Supercooling on Crystallization of Polyamide 11. *Macromolecules* **2013**, *46*, 828−835.
(58) Abdelsamie, M.; Treat, N. D.; Zhao, K.; McDowell, C.; Burgers, M. A.; Li, R.; Smilgies, D.-M.; Stingelin, N.; Bazan, G. C.; Amassian, A. Toward Additive-Free Small-Molecule Organic Solar Cells: Roles of the Donor Crystallization Pathway and Dynamics. *Adv. Mater.* **2015**, *27*, 7285−7292.
(59) Magill, J. H. Crystallization kinetics of polytetramethyl-P-silphenylene siloxane (TMPS) fractions. *J. Polym. Sci., Part B: Polym. Lett.* **1968**, *6*, 853−857.
(60) Xie, R.; Lee, Y.; Aplan, M. P.; Caggiano, N. J.; Muller, C.; Colby, R. H.; Gomez, E. D. Glass transition temperature of conjugated polymers by oscillatory shear rheometry. *Macromolecules* **2017**, *50*, 5146−5154.
(61) Sharma, A.; Pan, X.; Campbell, J. A.; Andersson, M. R.; Lewis, D. A. Unravelling the Thermomechanical Properties of Bulk Heterojunction Blends in Polymer Solar Cells. *Macromolecules* **2017**, *50*, 3347−3354.
(62) Sharma, A.; Pan, X.; Bjuggren, J. M.; Gedefaw, D.; Xu, X.; Kroon, R.; Wang, E.; Campbell, J. A.; Lewis, D. A.; Andersson, M. R. Probing the Relationship between Molecular Structures, Thermal Transitions, and Morphology in Polymer Semiconductors Using a Woven Glass-Mesh-Based DMTA Technique. *Chem. Mater.* **2019**, *31*, 6740−6749.
(63) Stingelin-Stutzmann, N.; Smits, E.; Wondergem, H.; Tanase, C.; Blom, P.; Smith, P.; de Leeuw, D. Organic thin-film electronics from vitreous solution-processed rubrene hypereutectics. *Nat. Mater.* **2005**, *4*, 601−606.
(64) Leman, D.; Kelly, M. A.; Ness, S.; Engmann, S.; Herzing, A.; Snyder, C.; Ro, H. W.; Kline, R. J.; DeLongchamp, D. M.; Richter, L. J. In Situ Characterization of Polymer−Fullerene Bilayer Stability. *Macromolecules* **2015**, *48*, 383−392.
(65) Li, G.; Shrotriya, V.; Huang, J.; Yao, Y.; Moriarty, T.; Emery, K.; Yang, Y. High-efficiency solution processable polymer photo-

https://doi.org/10.1021/acs.macromol.1c00296
Macromolecules 2021, 54, 5304−5320

voltaic cells by self-organization of polymer blends. *Nat. Mater.* **2005**, *4*, 864−868.
(66) Labram, J. G.; Domingo, E. B.; Stingelin, N.; Bradley, D. D.; Anthopoulos, T. D. In-Situ Monitoring of the Solid-State Microstructure Evolution of Polymer: Fullerene Blend Films Using Field-Effect Transistors. *Adv. Funct. Mater.* **2011**, *21*, 356−363.
(67) Beiner, M. Nanoconfinement as a tool to study early stages of polymer crystallization. *J. Polym. Sci., Part B: Polym. Phys.* **2008**, *46*, 1556−1561.
(68) Martín, J.; Mijangos, C. Tailored Polymer-Based Nanofibers and Nanotubes by Means of Different Infiltration Methods into Alumina Nanopores. *Langmuir* **2009**, *25*, 1181−1187.
(69) Mijangos, C.; Hernández, R.; Martín, J. A review on the progress of polymer nanostructures with modulated morphologies and properties, using nanoporous AAO templates. *Prog. Polym. Sci.* **2016**, *54*−*55*, 148−182.
(70) Fischer, F. S. U.; Tremel, K.; Sommer, M.; Crossland, E. J. C.; Ludwigs, S. Directed crystallization of poly(3-hexylthiophene) in micrometre channels under confinement and in electric fields. *Nanoscale* **2012**, *4*, 2138−2144.
(71) Martín, J.; Dyson, M.; Reid, O. G.; Li, R.; Nogales, A.; Smilgies, D.-M.; Silva, C.; Rumbles, G.; Amassian, A.; Stingelin, N. On the Effect of Confinement on the Structure and Properties of Small-Molecular Organic Semiconductors. *Adv. Electron. Mater.* **2018**, *4*, 1700308.
(72) Kouijzer, S.; Michels, J. J.; van den Berg, M.; Gevaerts, V. S.; Turbiez, M.; Wienk, M. M.; Janssen, R. A. J. Predicting Morphologies of Solution Processed Polymer:Fullerene Blends. *J. Am. Chem. Soc.* **2013**, *135*, 12057−12067.
(73) Müller, C.; Ferenczi, T. A. M.; Campoy-Quiles, M.; Frost, J. M.; Bradley, D. D. C.; Smith, P.; Stingelin-Stutzmann, N.; Nelson, J. Binary Organic Photovoltaic Blends: A Simple Rationale for Optimum Compositions. *Adv. Mater.* **2008**, *20*, 3510−3515.
(74) Zhao, J.; Swinnen, A.; Van Assche, G.; Manca, J.; Vanderzande, D.; Mele, B. V. Phase Diagram of P3HT/PCBM Blends and Its Implication for the Stability of Morphology. *J. Phys. Chem. B* **2009**, *113*, 1587−1591.
(75) Yang, X.; vanDuren, J. K. J.; Rispens, M. T.; Hummelen, J. C.; Janssen, R. A. J.; Michels, M. A. J.; Loos, J. Crystalline Organization of a Methanofullerene as Used for Plastic Solar-Cell Applications. *Adv. Mater.* **2004**, *16*, 802−806.
(76) Roozeboom, H. W. B. Erstarrungspunkte der Mischkrystalle zweier Stoffe. *Z. Phys. Chem.* **1899**, *30U*, 385−412.
(77) Vogel, R. Über eutektische Kristallisation. *Z. Anorg. Chem.* **1912**, *76*, 425−436.
(78) Smith, P.; Pennings, A. J. Eutectic crystallization of pseudo binary systems of polyethylene and high melting diluents. *Polymer* **1974**, *15*, 413−419.
(79) Yang, X.; Loos, J.; Veenstra, S. C.; Verhees, W. J. H.; Wienk, M. M.; Kroon, J. M.; Michels, M. A. J.; Janssen, R. A. J. Nanoscale Morphology of High-Performance Polymer Solar Cells. *Nano Lett.* **2005**, *5*, 579−583.
(80) Shaheen, S. E.; Brabec, C. J.; Sariciftci, N. S.; Padinger, F.; Fromherz, T.; Hummelen, J. C. 2.5% efficient organic plastic solar cells. *Appl. Phys. Lett.* **2001**, *78*, 841−843.
(81) Ma, W.; Yang, C.; Gong, X.; Lee, K.; Heeger, A. J. Thermally Stable, Efficient Polymer Solar Cells with Nanoscale Control of the Interpenetrating Network Morphology. *Adv. Funct. Mater.* **2005**, *15*, 1617−1622.
(82) Yu, G.; Gao, J.; Hummelen, J. C.; Wudl, F.; Heeger, A. J. Polymer Photovoltaic Cells: Enhanced Efficiencies via a Network of Internal Donor-Acceptor Heterojunctions. *Science* **1995**, *270*, 1789−1791.
(83) Halls, J. J. M.; Walsh, C. A.; Greenham, N. C.; Marseglia, E. A.; Friend, R. H.; Moratti, S. C.; Holmes, A. B. Efficient photodiodes from interpenetrating polymer networks. *Nature* **1995**, *376*, 498−500.
(84) Flory, P. J. *Principles of Polymer Chemistry*; Cornell University Press: Ithaca, NY, 1953.
(85) Mayer, A. C.; Toney, M. F.; Scully, S. R.; Rivnay, J.; Brabec, C. J.; Scharber, M.; Koppe, M.; Heeney, M.; McCulloch, I.; McGehee, M. D. Bimolecular Crystals of Fullerenes in Conjugated Polymers and the Implications of Molecular Mixing for Solar Cells. *Adv. Funct. Mater.* **2009**, *19*, 1173−1179.
(86) Jamieson, F. C.; Domingo, E. B.; McCarthy-Ward, T.; Heeney, M.; Stingelin, N.; Durrant, J. R. Fullerene crystallisation as a key driver of charge separation in polymer/fullerene bulk heterojunction solar cells. *Chem. Sci.* **2012**, *3*, 485−492.
(87) Shinohara, A.; Pan, C.; Guo, Z.; Zhou, L.; Liu, Z.; Du, L.; Yan, Z.; Stadler, F. J.; Wang, L.; Nakanishi, T. Viscoelastic Conjugated Polymer Fluids. *Angew. Chem., Int. Ed.* **2019**, *58*, 9581−9585.
(88) Babel, A.; Zhu, Y.; Cheng, K.-F.; Chen, W.-C.; Jenekhe, S. A. High Electron Mobility and Ambipolar Charge Transport in Binary Blends of Donor and Acceptor Conjugated Polymers. *Adv. Funct. Mater.* **2007**, *17*, 2542−2549.
(89) Todor-Boer, O.; Petrovai, I.; Tarcan, R.; Vulpoi, A.; David, L.; Astilean, S.; Botiz, I. Enhancing Photoluminescence Quenching in Donor−Acceptor PCE11:PPCBMB Films through the Optimization of Film Microstructure. *Nanomaterials* **2019**, *9*, 1757.
(90) Alam, M. M.; Tonzola, C. J.; Jenekhe, S. A. Nanophase-Separated Blends of Acceptor and Donor Conjugated Polymers. Efficient Electroluminescence from Binary Polyquinoline/Poly(2-methoxy-5-(2-ethylhexyloxy)-1,4-phenylenevinylene) and Polyquinoline/Poly(3-octylthiophene) Blends. *Macromolecules* **2003**, *36*, 6577−6587.
(91) Radano, C. P.; Scherman, O. A.; Stingelin-Stutzmann, N.; Müller, C.; Breiby, D. W.; Smith, P.; Janssen, R. A. J.; Meijer, E. W. Crystalline-crystalline block copolymers of regioregular poly(3-hexylthiophene) and polyethylene by ring-opening metathesis polymerization. *J. Am. Chem. Soc.* **2005**, *127*, 12502−12503.
(92) Xie, X.; Xu, C.; Wang, G.; Dong, J.; Cao, W.-D.; Kennedy, R. TTT Diagram of a Newly Developed Nickel-Base Superalloy−Allvac® 718Plus. *Superalloys* **2005**, *718*, 706.
(93) Enomoto, M. Prediction of TTT-diagram of proeutectoid ferrite reaction in iron alloys from diffusion growth theory. *ISIJ. Int.* **1992**, *32*, 297−305.
(94) Oradei-Basile, A.; Radavich, J. F. A current TTT diagram for wrought alloy 718. *Superalloys* **1991**, *718*, 325−335.
(95) Yu, L.; Davidson, E.; Sharma, A.; Andersson, M. R.; Segalman, R.; Müller, C. Isothermal Crystallization Kinetics and Time−Temperature−Transformation of the Conjugated Polymer: Poly(3-(2′-ethyl)hexylthiophene). *Chem. Mater.* **2017**, *29*, 5654−5662.
(96) Kuei, B.; Gomez, E. D. Chain conformations and phase behavior of conjugated polymers. *Soft Matter* **2017**, *13*, 49−67.
(97) Goffri, S.; Müller, C.; Stingelin-Stutzmann, N.; Breiby, D. W.; Radano, C. P.; Andreasen, J. W.; Thompson, R.; Janssen, R. A. J.; Nielsen, M. M.; Smith, P.; Sirringhaus, H. Multicomponent semiconducting polymer systems with low crystallization-induced percolation threshold. *Nat. Mater.* **2006**, *5*, 950−956.
(98) Scaccabarozzi, A. D.; Basham, J. I.; Yu, L.; Westacott, P.; Zhang, W.; Amassian, A.; McCulloch, I.; Caironi, M.; Gundlach, D. J.; Stingelin, N. High-density polyethylene—an inert additive with stabilizing effects on organic field-effect transistors. *J. Mater. Chem. C* **2020**, *8*, 15406−15415.
(99) Kumar, A.; Baklar, M. A.; Scott, K.; Kreouzis, T.; Stingelin-Stutzmann, N. Efficient, Stable Bulk Charge Transport in Crystalline/Crystalline Semiconductor−Insulator Blends. *Adv. Mater.* **2009**, *21*, 4447−4451.
(100) Ferenczi, T. A. M.; Müller, C.; Bradley, D. D. C.; Smith, P.; Nelson, J.; Stingelin, N. Organic Semiconductor:Insulator Polymer Ternary Blends for Photovoltaics. *Adv. Mater.* **2011**, *23*, 4093−4097.

https://doi.org/10.1021/acs.macromol.1c00296
Macromolecules 2021, 54, 5304−5320